Effect of Surface Moisture Condition on Substrate-Repair Concrete Overlay Transition Zone

Douglas M. Annand

Thesis submitted to the faculty of the Virginia Polytechnic Institute and State University in partial fulfillment of the requirements for the degree of

Master of Science

In

Civil Engineering

Alexander S. Brand, Chair
Gerardo W. Flintsch
Scott W. Case

December 8, 2022
Blacksburg, VA

Keywords: concrete repair, interfacial transition zone (ITZ), overlay transition zone (OTZ), substrate moisture condition, X-ray computed tomography (XCT), freeze/thaw conditions, dental X-ray.

Effect of Surface Moisture Condition on Substrate-Repair Concrete Overlay Transition Zone

Douglas M. Annand

ACADEMIC ABSTRACT

Concrete is the most widely used construction material in the world. Given its relative availability, strength, economy, and versatility to fit various applications, the material has been incorporated in roadways, bridges, buildings, and a host of other infrastructure projects. Oftentimes, concrete will be exposed to several environmental conditions that ultimately affect its durability and lifespan. These conditions include repeated freezing and thawing, chloride intrusion, sulfate attack, alkali-silica reaction, and many others.

Given the age and condition of American infrastructure, concrete structures throughout the country need repair or rehabilitation. Often this repair includes the removal of degraded or damaged concrete and the application of an overlay material. There are several factors affecting the bond performance of the newly formed substrate-repair concrete, such as surface roughness, overlay material, and substrate moisture condition. The work presented in this thesis is dedicated to understanding the effect of substrate moisture condition on the overlay transition zone (OTZ) of the substrate-repair concrete. The substrate moisture condition can significantly impact the microstructure characterization of the OTZ. If the substrate is too dry, then it may absorb water from the repair material, reducing the local water-to-cement (w/c) ratio in the OTZ. Conversely, if the substrate is too wet, then the w/c ratio of the OTZ will be locally increased. In both scenarios, the interfacial bond strength is expected to be modified due to the change in the local w/c ratio. To understand this effect, various test methods and degradation mechanisms were explored. Initially, substrate-repair concrete specimens were prepared utilizing three separate substrate moisture conditions: saturated surfaced dry (SSD), sub-saturated surface dry (Sub-SSD), and oven dry (OD). After allowing these samples to cure, the strength and ion penetration risk were evaluated. The bond strength of the samples was evaluated through flexural strength testing and fracture energy determined through the RILEM draft tests. The OTZ ion penetration risk was evaluated by

conducting rapid chloride penetration test (RCPT) on samples prepared with the three substrate moisture conditions. Furthermore, to determine the effect of repeated freezing and thawing on the OTZ and flexural strength, additional samples were created with the three moisture conditions. After allowing these samples to cure, they were subjected to ASTM C666 and were tested to observe their flexural strength.

Another important performance indicator of concrete elements is its resistance to chloride ion penetration and corrosion. Since many structural elements are designed with steel reinforcement, chloride ion penetration represents a critical parameter in projecting material performance, since chloride ions will accelerate the rate of steel corrosion. Oftentimes, a key element in projecting this performance is identifying the rate at which ions diffuse through the material. There remain many established techniques to identify this rate of diffusion and derive a chloride diffusion coefficient; however, many of them are either destructive or qualitative in nature. In recent years, transmission X-ray microscopy (TXM) has been employed to non-destructively track diffusion and develop diffusion coefficients. The work presented in this thesis surrounds the efforts of incorporating TXM experiments at Virginia Tech. This work initially utilized a SkyScan 1174 μCT, and additional work in this thesis presents the design and construction of a dental X-ray system based on the checking ion penetration (CHIP) design. This system can conduct TXM experiments utilizing a dental X-ray as the source. The research, design, and construction of the CHIP system is discussed in this thesis.

Ultimately, the research in this thesis has not observed any significant relationship between substrate moisture condition and overlay bond strength. There does appear to be an increase in chloride ion resistance for drier substrates, suggesting that pre-wetting the surface increases penetrability of the interface.

Effect of Surface Moisture Condition on Substrate-Repair Concrete Overlay Transition Zone

Douglas M. Annand

GENERAL AUDIENCE ABSTRACT

Concrete is the most widely used construction material in the world. Given its relative availability, strength, economy, and versatility to fit various applications, the material has been incorporated in roadways, bridges, buildings, and a host of other infrastructure projects. Oftentimes, concrete will be exposed to several environmental conditions that ultimately affect its durability and lifespan. These conditions include repeated freezing and thawing, chloride intrusion, sulfate attack, alkali-silica reaction, and many others. These environmental conditions ultimately degrade the material by inducing cracks, exposing steel reinforcement, and spalling. When the concrete has experienced significant deterioration, repair and rehabilitation of the damaged section must be performed. Most often, this repair consists of the removal of damaged concrete and the application of an overlay material to prevent further deterioration. The topics discussed in this thesis evaluate the optimum substrate conditions prior to an overlay application and the implementation of techniques to evaluate deterioration mechanisms. There are several substrate conditions that will affect bonding with the overlay material, including surface roughness, moisture conditions, and overlay type. This paper focused on the moisture condition and what effect this had on bond strength and resistance to chloride intrusion. This effect was studied in laboratory conditions and under environmental conditions such as rapid freezing and thawing. Several different deterioration mechanisms may contribute to concrete degradation. The research presented in this thesis also aimed to evaluate chloride ion diffusion. To evaluate this mechanism, two systems were explored with the intent of conducting transmission X-ray microscopy (TXM). With TXM, chloride ion diffusion can be tracked to determine the rate at which ions diffuse through the concrete. The two systems explored were an X-ray computed tomography scanner and a dental X-ray system. Both systems can conduct TXM, and this paper presents the efforts dedicated to developing them for this technique at Virginia Tech.

Ultimately, the research in this thesis has not observed any significant relationship between substrate moisture condition and overlay bond strength. There does appear to be an increase in chloride ion resistance for drier substrates, suggesting that pre-wetting the surface increases penetrability of the interface.

ACKNOWLEDGEMENTS

I want to extend my gratitude to my committee chair, Dr. Alexander Brand, for his assistance during my research and his support throughout my journey at Virginia Tech. I would also like to thank Drs. Scott Case and Gerardo Flintsch for serving on my committee and providing their expertise and support.

Additionally, I want to demonstrate my tremendous appreciation to the faculty and staff at the structures laboratory for their assistance in completing projects discussed in this thesis. The support of Dr. David Mokarem, Brett Farmer, and Garret Blankenship was vital to the completion of my research and their knowledge was always appreciated. I would also like to thank the students of the Brand Research Group for their support along the way. They were always willing to lend an extra hand or an ear to discuss ideas. Lastly, I would like to thank Paul Atwood for his tireless efforts over the summer while we prepared most of the samples tested in this thesis.

Finally, I want to express my admiration to my family, especially my wife Candice, for their support during my studies. There have been academic challenges, the birth of our daughters, and cross-country moves along this journey, but support for my academic endeavors has remained steadfast. I simply would not be here without their support.

Table of Contents

1. Introduction 1

1.1 Objectives and Scope 1

1.2 Organization of Thesis 3

2. Literature Review 5

2.1 Substrate-Repair Concrete 5

2.2 Transmission X-ray Microscopy 17

2.3 Freeze/Thaw Conditions on Substrate-Repair Concrete 30

3. Section 1: Substrate-Repair Concrete 39

3.1 Background 39

3.2 Methods and Procedures 41

3.3 Results and Discussion 51

3.4 Conclusions 67

3.5 Future Work 69

4. Section 2: X-Ray Computed Tomography (XCT) and Dental X-Ray (CHIP) 71

4.1 Background 71

4.2 Methods and Procedures 73

4.3 Results and Discussion 76

4.4 Conclusions 85

4.5 Future Work 86

5. Section 3: Freeze/Thaw Conditions on Substrate-Repair Concrete 87

5.1 Background 87

5.2 Methods and Procedures 87

5.3 Results and Discussion 89

5.4 Conclusions 93

5.5 Future Work 93

6. Conclusions and Future Work 95

Appendix A 97

References 99

List of Figures

Figure 1: The "Wall Effect" [2] 6

Figure 2: Gradation by Zone Due to the "Wall Effect" [2] 6

Figure 3: Effect of RCA on Compressive Strength at 28 Days [4] 7

Figure 4: Effect of RCA on Tensile Strength at 28 Days [4] 8

Figure 5: Influence of Overlay Strength and Substrate Moisture Condition [1] 9

Figure 6: SEM Images of OTZ. a) M1, b) M3, c) M4 [1] 10

Figure 7: Image Analysis of OTZ: a) M1, b) M3, c) M4 [1] 10

Figure 8: Shear Bond Apparatus [7] 12

Figure 9: Shear Strength. Symbols: Dry Substrate (Solid); Pre-Wetted Substrate (Open) [7] 12

Figure 10: Phase Boundary Model [9] 14

Figure 11: SSD (Left), Dry (Right) Test Specimens. Bright White is Adhered Concrete [10] 15

Figure 12: Adhesion of Mortar. Mortar A (Top), Mortar B (Bottom) [11] 16

Figure 13: Time-Series Radiographs [23] 22

Figure 14: XRF and TXM I Concentration Comparison [23] 22

Figure 15: Comparison of I and KI Diffusion Coefficients [23] 23

Figure 16: Diffusion Coefficients at 20% FA Replacement [24] 24

Figure 17: Diffusion Coefficients at 40% FA Replacement [24] 24

Figure 18: Diffusion Coefficients and Porosity (%) [22] 25

Figure 19: Depth of Penetration [22] 26

Figure 20: CHIP Schematic [25] 28

Figure 21: SkyScan 1172 µCT (L), CHIP (R) [25] 28

Figure 22: µCT vs CHIP Iodide Concentrations at Depth [25] 29
Figure 23: Silane Sealer vs. Iodide Concentration [25] 30
Figure 24: Freeze/Thaw Crack Propagation [26] 31
Figure 25: FT Cycle vs. Water Absorption and RDME [27] 32
Figure 26: FT Cycles vs. Porosity, Surface Area, and Volume [28] 33
Figure 27: Pore and Crack Evolution in ITZ [28] 34
Figure 28: FT Damage Rough Surface. 0-Cycles (L), 50-Cycles (R) [30] 35
Figure 29: FT Damage Smooth Surface. 0-Cycles (L), 50-Cycles (R) [30] 35
Figure 30: FT Cycles vs. Compressive and Pressure Tension [31] 36
Figure 31: FT Cycle vs. PT/CS Ratio [31] 37
Figure 32: Substrate-Repair Flexural Specimen 42
Figure 33: Failed Adhesion (10% RH). Substrate (Left), Repair (Right) 43
Figure 34: 3-Point Loading. ASTM C293 [42] 44
Figure 35: 4-Point Loading. ASTM C78 [43] 44
Figure 36: 3-Point Loading on Substrate Specimen 45
Figure 37: Fracture Prism 46
Figure 38: Induced Notch. Substrate (Left), Repair (Right) 46
Figure 39: RILEM TPFM Testing 47
Figure 40: RCPT Cylinder and Puck Schematic 49
Figure 41: RCPT Cylinders (80% RH); Substrate (S), Repair (R) 49
Figure 42: RCPT Vacuum Chamber 50
Figure 43: RCPT System 50

Figure 44: 98% RH Interface Adhesion. Repair (Left), Substrate (Right) 55

Figure 45: 98% RH Interface Aggregate. Repair (Left), Substrate (Right) 55

Figure 46: Substrate Fracture Results 58

Figure 47: SSD (98% RH) Fracture Results 58

Figure 48: Sub-SSD (80% RH) Fracture Results 59

Figure 49: OD (10% RH) Fracture Results 59

Figure 50: 98% RH Fracture Plane. Repair (R), Substrate (L) 62

Figure 51: 80% RH Fracture Plane. Repair (L), Substrate (R) 62

Figure 52: 10% RH Fracture Plane. Repair (R), Substrate (L) 63

Figure 53: 80% RH Failed Puck 64

Figure 54: SkyScan 1174 μCT 71

Figure 55: XCT Calibration Samples 73

Figure 56: 3D Stage Design 74

Figure 57: 3D Filter Holder Design 75

Figure 58: XCT Samples with Wax and PVC Nut 76

Figure 59: 0% (Left) and 10% (Right) KI Radiographs 77

Figure 60: Time-Series Radiograph [16] 77

Figure 61: 0% (Left) and 10% (Right) KI Radiographs – 2nd Attempt 78

Figure 62: 0% (Left) and 10% (Right) KI Radiographs with Filter– 3rd Attempt 79

Figure 63: 14-Day Radiograph. M1-1 (Left), M1-2 (Right) 80

Figure 64: 14-Day Radiograph, T1-1 (Left), T1-2 (Right) 80

Figure 65: 5-Day Radiograph, Concrete Core 80

Figure 66: Sample T1-1 Time-Series Radiograph, Option 3 81

Figure 67: Sample T1-1 Time-Series Radiograph, Option 4 82

Figure 68: CHIP System Schematic 84

Figure 69: CHIP System (Outside) 85

Figure 70: CHIP System. Panel (L), X-ray Source (R) 85

Figure 71: 10% RH Prism after FT 89

Figure 72: 98% RH Prism after FT 89

Figure 73: Substrate Cylinder after FT (Top) 89

Figure 74: Substrate Cylinders after FT (Side) 90

Figure 75: XCT Stage (Top) 97

Figure 76: XCT Stage (Bottom) 97

Figure 77: XCT Stage (Side) 98

Figure 78: Filter Holder (Side) 98

Figure 79: Filter Holder (Front) 98

List of Tables

Table 1: Concrete Mix Design for $1yd^3$ 39

Table 2: Material Properties 41

Table 3: 3-Point Flexural Testing Results 51

Table 4: 3-Point Substrate Moisture Comparison 52

Table 5: 4-Point Flexural Testing Results 53

Table 6: 4-Point Substrate Moisture Comparison 53

Table 7: RILEM Fracture Results 60

Table 8: Average RILEM Fracture Results 61

Table 9: Initial RCPT Results 65

Table 10: Chloride Ion Penetrability Risk Based on Charge Passed (C) 65

Table 11: RCPT Retest Results 66

Table 12: RCPT Average Results 66

Table 13: Cement Mortar Mix Design 72

Table 14: Cement Mortar Mix Design - Final Trial 83

Table 15: Compressive Strength after FT 90

Table 16: 3-Point Flexural Testing Results after Freeze/Thaw 91

Table 17: Freeze/Thaw Flexural Testing Comparison 91

Table 18: Freeze/Thaw Flexural Testing Results Comparison 92

1. Introduction

This section is reserved to introduce the thesis. It will contain two sections, Objectives and Scope, and the Organization of Thesis. The Objectives and Scope section will outline the main goal of the research contained within. The Organization of Thesis will outline what each chapter will contain.

1.1 Objectives and Scope

Concrete is the most widely used construction material in the world. Given its relative availability, strength, economy, and its workability to fit various applications, the material has been incorporated in roadways, bridges, buildings, and a host of other infrastructure projects. Oftentimes, concrete will be exposed to several environmental conditions, ultimately affecting its durability and lifespan. These conditions include freezing and thawing, chloride intrusion, sulfate attack, alkali-silica reaction, and many others. Understanding these degradation mechanisms, how they affect concrete, and developing solutions at mitigating deterioration is of upmost importance, given the C– rating of America's infrastructure by the American Society of Civil Engineers. The bulk of the research contained in this thesis will be evaluating these degradation mechanisms and researching the repair methodologies utilized to correct them. Since this thesis will discuss the efforts involved with three separate projects, objectives and scope will be defined for each.

In the first project, the research efforts are dedicated to understanding the effect of substrate moisture condition on the overlay transition zone (OTZ) between substrate and repair concrete. This substrate-repair bond is developed when a concrete structure has experienced degradation severe enough to justify rehabilitation. This repair will include the casting of new concrete along the damaged substrate to prevent further degradation. As identified by previous researchers, the OTZ between the substrate-repair concrete will be the weakest portion of the newly formed matrix. As such, this project evaluated the flexural strength, fracture energy, and the chloride ion penetrability risk of this region. To understand the extent substrate moisture condition has on these properties, various substrate moisture conditions were

generated prior to forming the substrate-repair concrete, including saturated surface dry (SSD), sub-saturated surface dry (Sub-SSD), and oven dry (OD).

For most structural applications, concrete elements are reinforced with steel rebar to increase the tensile capacity of the material. Since many concrete elements are exposed to environmental conditions, they are often at-risk of developing corrosion. Chloride ingress, such as from deicing chemicals or seawater, is particularly of concern since chloride ions will accelerate the rate of corrosion of steel reinforcement. The rate of penetration of chloride ions into the concrete is a unique parameter specific to each concrete mix, so the rate at which ions diffuse through the concrete needs to be quantified. Therefore, the research presented in this thesis outlines two techniques employed for evaluating chloride ion diffusion in concrete: X-ray computed tomography (XCT) and a dental X-ray system based on the checking ion penetration (CHIP) design. These techniques are similar in methodologies but represent two different approaches laboratories may take to evaluate chloride diffusion in their facilities. For the XCT portion of this thesis the efforts were directed to revitalizing the in-house SkyScan 1174 micro XCT scanner and, if operable, perform transmission X-ray microscopy (TXM) to evaluate chloride ion diffusion. The CHIP system is similar in that it employs TXM to evaluate chloride ion diffusion, but this system is designed and built in the laboratory utilizing dental X-ray equipment. This projects' focus was to research, design, and construct a CHIP system at Virginia Tech.

The final efforts of this thesis were to evaluate the combined effects of substrate moisture condition and freeze/thaw (FT) environments on concrete. As stated above, the OTZ between substrate-repair concrete is its weakest region. It is also known that repeated freezing and thawing of concrete generates microstructure cracking which leads to spalling and exposure of the steel reinforcement. Since FT can have significant impacts on the performance and lifespan of concrete elements, the United States Army Corps of Engineers (USACE) is interested in further evaluating and understanding these effects. Therefore, this research project was aimed at understanding the effect of substrate moisture condition on elements exposed to FT environments. To evaluate the effects, samples were created with various

substrate moisture conditions and then subjected to FT conditions. Afterwards, the samples were tested to see the significance substrate moisture condition had on the sample's strength.

1.2 Organization of Thesis

This thesis is the culmination of several projects conducted to evaluate the overlay transition zone (OTZ) of substrate-repair concrete in regular field conditions, the OTZ in substrate-repair concrete specimens subjected to freezing and thawing cycles, and the utilization of XCT to evaluate chloride ion diffusion. As a result, this thesis is divided into sections to discuss methods and procedures utilized in each project.

Chapter 1 of the thesis introduces the topics contained within the thesis, to include project objectives and scope. Additionally, this section provides an overview of the organization of thesis and projects.

Chapter 2 of the thesis provides a literature review for each of the research projects. This chapter introduces each project in a separate subsection where the pertinent published literature will be reviewed. This literature review will provide the basis for the research and be utilized to outline current knowledge and accepted information.

Chapter 3 discusses the evaluation of the OTZ of substrate-repair concrete to identify the optimum substrate surface moisture content. To discuss this project, the chapter is divided into several subsections, including Background, Methods and Procedures, Results and Discussion, Conclusions and Future Work. These sections are aimed at providing a brief description of the intent of the project, outlining creation of the specimens, testing procedures, determined results with their conclusions, and a discussion of possible future work.

Chapter 4 of the thesis presents a discussion on utilizing X-rays to obtain radiographs and non-destructively evaluating chloride ion diffusion. For this research, two approaches were utilized. The first approach was to utilize a SkyScan 1174 micro XCT scanner and the second was the design and

development of the CHIP system, using a dental X-ray source. As such, this chapter is split into two sections and will identify the outcome of each approach.

Chapter 5 presents the OTZ evaluation of substrate-repair concrete subject to rapid freezing and thawing. Like Chapter 2, this section is separated into the following sections: Background, Methods and Procedures, Results and Discussion, Conclusions, and Future Work.

Chapter 6 is the final chapter of the thesis and presents conclusions and recommendations for future works.

2. Literature Review

This section is reserved to provide a literature review for the projects contained within this thesis. As such, each of the three projects will be separated into subsections within the chapter.

2.1 Substrate-Repair Concrete

The serviceability of a concrete structure can be affected by many deterioration mechanisms. These mechanisms include overloading, alkali-silica reaction, chloride intrusion, corrosion, and many other environmental influences. A structure will exhibit deterioration in various forms, including delamination, cracking, and spalling. When this deterioration progresses, structures will require some sort of repair or rehabilitation. Oftentimes, this repair will require the removal of the defective or deteriorated concrete and the application of an overlay material to prevent future intrusion and damage. When the new material is applied to the existing substrate, the region between the substrate and repair material is of most importance. Formally, this region is identified as the overlay transition zone (OTZ) and is characterized by higher porosity, higher cement paste content (compared to the bulk concrete), and increased air voids [1]. As a result, the OTZ will represent the weakest portion of the substrate-repair concrete and will be the focus of this project.

The OTZ is a region analogous to the interfacial transition zone (ITZ) that was originally identified as the region around an aggregate in a concrete matrix. The ITZ is characterized by a zone of high porosity and cement paste content that develops in a region of approximately 15-20 μm around an aggregate [2]. This region is formed due to what is called “the wall effect”, which is created due to the inefficient packing of cement particles against an aggregate. As a result, large cement particles are unable to efficiently orient around the aggregate and a greater concentration of smaller cement grains form along the ITZ. *Figure 1* displays a representation of the wall effect.

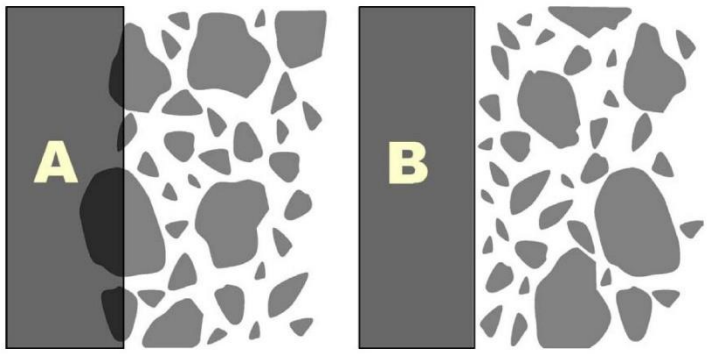

Figure 1: The "Wall Effect" [2]

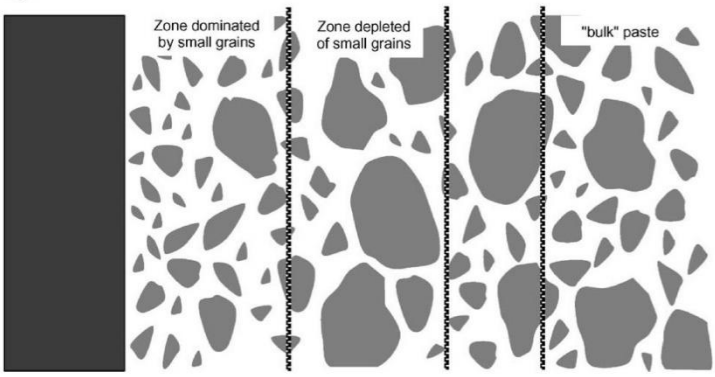

Figure 2: Gradation by Zone Due to the "Wall Effect" [2]

On the left, labeled “A” is the ideal particle packing distribution where large cement grains can “cut through” the solid surface and generate a well-graded distribution around an aggregate. On the right, labeled “B” is the actual distribution where large cement particles are unable to efficiently pack around the aggregate and a large concentration of smaller cement particles form. In *Figure 2*, a schematic is displayed showing the gradation of cement grains in separate zones, extending away from the aggregate. It shows that as the distance from the aggregate increases, the cement particles can more efficiently consolidate and achieve uniform distribution. This inefficient particle packing is the reason for the increase in porosity and a decrease in strength of the ITZ relative to the bulk microstructure.

As a result of the loss of mechanical properties and durability in this region, published literature has evaluated the OTZ of substrate-repair concrete to identify best construction practices aimed at mitigating the effects. In the field, the current best practices recommend thoroughly cleaning the substrate of all deteriorated concrete and pre-wetting the surface prior the application of any overlay [3]. This practice was developed due to the importance of sufficient water needed for hydration of cement particles

in the repair material. It is believed a substrate not pre-wetted will be overly dry and as a result, will absorb the water from the repair material. The loss of water in the repair material will inhibit the hydration reaction necessary for adequate adhesion in the bond. Unfortunately, published literature has not provided a consensus on the optimum level of substrate surface moisture condition because the level of moisture will have varying effects depending on the properties being measured.

As a corollary, researchers have studied the ITZ for recycled concrete aggregates (RCA) in mortar and concrete. In one study it was determined RCA with pre-wetted aggregates displayed a reduction in compressive and splitting tensile strengths and the best performance was exhibited by the dry aggregates [4]. The increase in strength is attributable to the dry aggregates' absorption of the mixing water, locally reducing the water-to-cement (w/c) ratio and generating a stronger concrete matrix. *Figure 3* displays the relationship between recycled aggregate content, compressive strength, and recycled aggregate moisture content. The graph demonstrates two key findings:

1. Effect of moisture content on strength: except for a 60% RCA replacement, the dry aggregates achieved greater strength than pre-wetted aggregates for all replacement ratios.
2. RCA's effect on compressive strength – with 20% and 40% RCA, there is an increase in compressive strength when compared to mixes utilizing virgin aggregates.

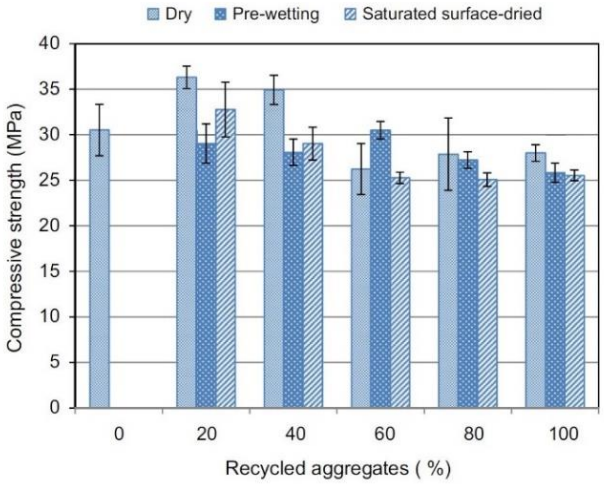

Figure 3: Effect of RCA on Compressive Strength at 28 Days [4]

Similar findings were discovered when evaluating the tensile strength of the same concrete mixes. *Figure 4* displays the relationship between recycled aggregate content, tensile strength, and recycled aggregate moisture content. These results are comparable to the observations in compressive strength testing and produced similar key findings:

1. Effect of moisture content on strength: except for 60% and 80% RCA replacements, the dry aggregates achieved greater strength than pre-wetted aggregates for all replacement ratios.
2. RCA effect on tensile strength – with 20% RCA, there is an increase in tensile strength when compared to mixes utilizing virgin aggregates.

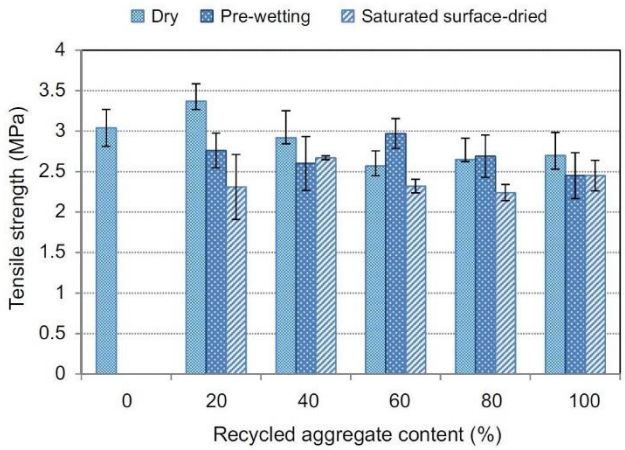

Figure 4: Effect of RCA on Tensile Strength at 28 Days [4]

These results demonstrate the optimum surface moisture condition for RCA utilized in an RAC mix is the dry condition. The authors have attributed this performance to a locally reduced w/c ratio along the ITZ because of the absorption of mixing water by the RCA. However, other studies have explicitly shown that the quality of the ITZ of oven-dry RCA is worse than that of saturated RCA [5, 6].

Furthermore, published literature evaluating the OTZ of substrate-repair concrete utilized in repairs has demonstrated a similar reduction in performance when substrates are pre-wetted. One study evaluated the OTZ of substrate-repair concrete utilizing varying strengths of substrate concrete [1]. The researchers evaluated the substrate-repair bond strength utilizing four separate moisture conditions:

1. Saturated Surface Dry (M1): substrates submerged for 24 hours.
2. Saturated Surface Dry (M2): substrates submerged for 30 minutes prior to repair material application.
3. Dry Substrate (M3): substrates stored at room temperature and humidity.
4. Oven Dry Substrate (M4): substrates dried in an oven for 24 hours.

They determined pre-wetting did not provide a statistically significant improvement on the bond strength of the OTZ, regardless of the strength of the substrate and overlay concretes. The authors concluded pre-wetting the substrate increased the porosity of the bond and ultimately reduced its strength. *Figure 5* compares the four substrate moisture conditions to the shear strength and demonstrates that the dry substrate (M3) and oven dry substrate (M4) outperformed the saturated surface dry specimens (M1).

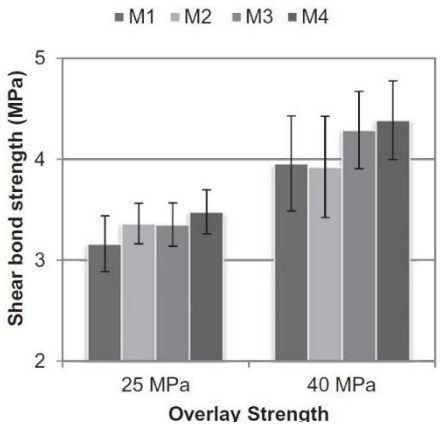

Figure 5: Influence of Overlay Strength and Substrate Moisture Condition [1]

The authors observed an increase in paste content and porosity along the OTZ for substrates that were pre-wetted and attribute the overall reduction in shear bond strength to this observation. To quantify this observation, they performed a microstructure evaluation on the OTZ utilizing a scanning electron microscope (SEM) to image the region. The SEM images obtained for three of the moisture conditions are displayed in *Figure 6.*

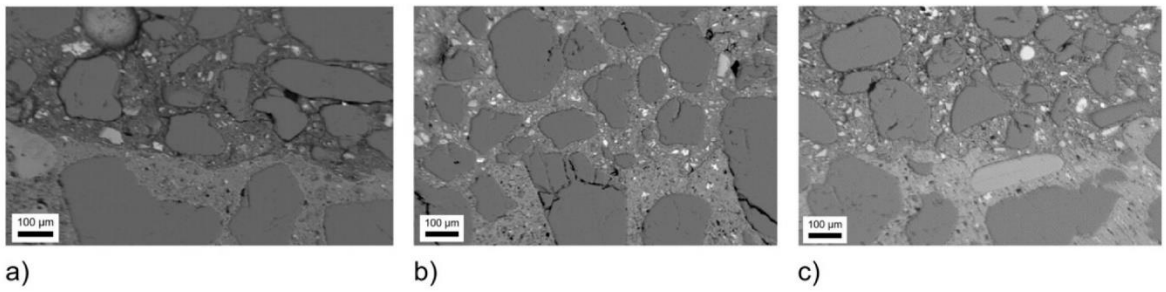

Figure 6: SEM Images of OTZ. a) M1, b) M3, c) M4 [1]

The OTZ of the substrate-repair concrete can be clearly identified from the SEM images. *Figure 6* displays the overlay material on top, with the substrate on bottom, separated by the OTZ—identified by a thin layer of hardened paste and anhydrous cement. The OTZ is more easily identified in the saturated surface dry specimen (M1) by its lack of large aggregates. An increased concentration of large aggregates can be seen by viewing the SEM image of the oven dry substrate (M4). To quantify the content of anhydrous cement, pores, aggregates, and hardened paste along the OTZ, the authors also performed an image analysis of the obtained SEM images. The results of the analysis are displayed in *Figure 7*, where the percentage of each content is determined relative to the distance from the OTZ.

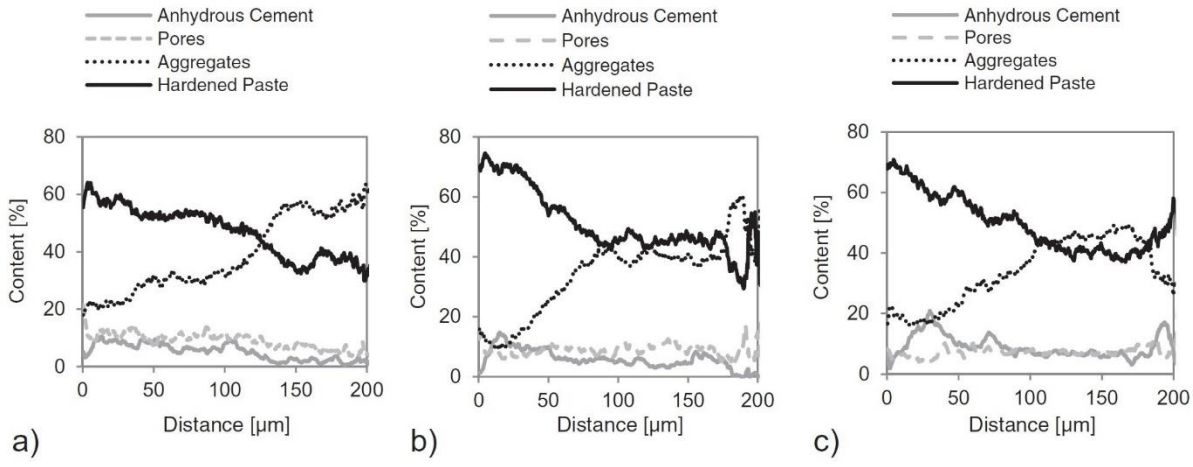

Figure 7: Image Analysis of OTZ: a) M1, b) M3, c) M4 [1]

From the image analysis the authors concluded that all moisture conditions demonstrated a high hardened paste content (60-70%) compared to aggregate content (20%). Additionally, from the images the authors observed an increase in pore content when substrates were pre-wetted and the specimen with the lowest content of pores were the oven dried specimens (M4). Ultimately, utilizing the SEM images and the image analysis, the authors were able to conclude that pre-wetting reduced the overall shear bond strength of the substrate-repair concrete due to an increase in porosity along the OTZ. These findings were consistent regardless of substrate and overlay material strength.

Additional published literature on the substrate-repair OTZ has supported the results of the previous study and concluded pre-wetting may have a negative effect on bond strength. One study evaluated the bond strength of substrate utilizing five different overlay materials with varying water-to-binder (w/b) ratios, producing eight different overlay materials that are outlined below [7]:

1. CEM I: portland cement concrete
2. SFC_1: silica fume concrete (w/b: 0.46)
3. SFC_2: silica fume concrete (w/b: 0.40)
4. SFC_3: silica fume concrete (w/b: 0.55)
5. CSC_1: Corex slag concrete (w/b: 0.40)
6. CSC_2: Corex slag concrete (w/b: 0.55)
7. PolyRep: polymer-modified repair mortar
8. CemRep: non-sag cement-based repair mortar

In this study the authors utilized two separate substrate moisture conditions to evaluate the bond strength: dry substrate and saturated surface dry (SSD) substrate. The dry substrate specimens were stored in normal laboratory conditions for a minimum of four weeks, while the SSD specimens were submerged in water 24 hours prior to the casting of the overlay material. To evaluate the shear bond strength of the OTZ, the authors subjected the test specimens to a shear force by utilizing the apparatus in *Figure 8*.

Figure 8: Shear Bond Apparatus [7]

After performing the test on all specimens, the authors concluded that pre-wetting the substrate prior to the application of the overlay material provided no additional benefit in shear strength. They noted that in all but two cases, the dry substrates demonstrated higher shear strength than substrates that were pre-wetted. A graphical representation of their findings is presented in *Figure 9.*

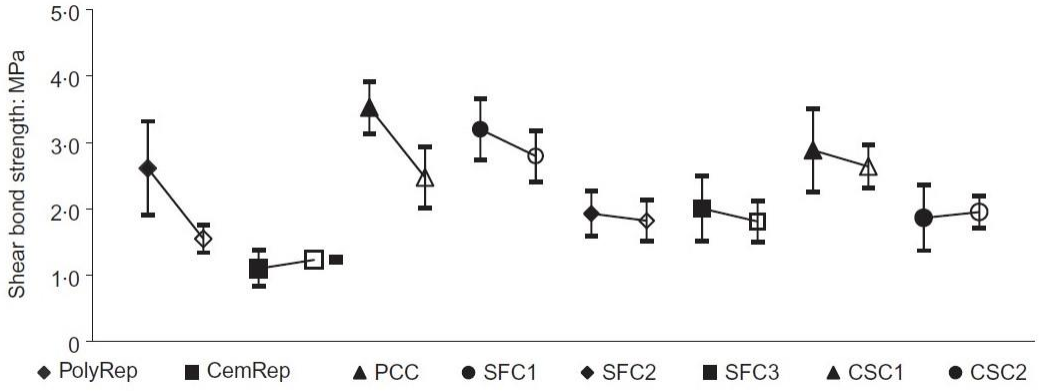

Figure 9: Shear Strength. Symbols: Dry Substrate (Solid); Pre-Wetted Substrate (Open) [7]

The authors also note that six of the eight overlay materials demonstrated proximity in shear bond strength between the dry and saturated surface dry substrates. The two exceptions to this were the PCC and PolyRep overlays which demonstrated a more significant decrease in shear bond strength when the substrates were pre-wetted. The authors explain that of the eight overlays tested, the PCC and PolyRep

overlay materials had the highest slump (increased workability) than the other materials. This increase in workability would allow the repair material to flow and fill the voids in the substrate more adequately. They conclude there may be a correlation between shear bond strength and repair material fluidity that is reducing the shear bond strength, but this conclusion would need further research.

Further studies have demonstrated similar results to those published above. In a study evaluating the OTZ of substrate-repair concrete for the application of overlay repair materials, the authors of "Concrete Substrate Moisture Requirements for Effective Concrete Repairs" utilized ponding as their means of obtaining substrate moisture condition. The authors subjected the specimens to three different ponding periods: no ponding, ponding for 1 hour, and ponding for 6 hours prior to the application of an overlay. The results of the study indicate that for normal and high strength concrete (greater than 5000 psi), pre-wetting provided no statistically significant increase in bond strength. However, for lower strength substrate, a ponding period of 6 hours was determined to achieve the best performance. Due to the varying strengths of in-situ concrete, the results of this study led the authors to conclude there is no optimum level of substrate moisture content that will satisfy all substrate and overlay materials [8].

The reduction of shear strength and mechanical properties in the ITZ between aggregate-cement particles has been experimentally demonstrated through the literature discussed in this review. To quantify this reduction in strength, other researchers have proposed a modeling system used to evaluate the ITZ in distinct regions identified in the *Figure 10* [9]. They proposed distinct, uniform regions surrounding an aggregate and evaluated the regions with a mathematical model to determine the effective shear and elastic moduli of the ITZ. The authors employ previously published experimental data of the shear modulus of mortar samples containing varying amounts of fine aggregate concentrations. Utilizing this data and their proposed model, the authors determined the shear and Young's moduli of the ITZ will be approximately 50% of that of the bulk cement paste matrix.

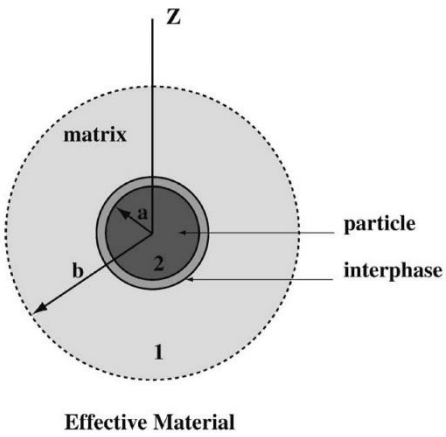

Figure 10: Phase Boundary Model [9]

Although the purpose of this literature review is mostly to discuss the optimum level of surface moisture content in the OTZ of substrate-repair concrete, the reduction of strength properties in the ITZ is analogous to this discussion. This modeled approach mentioned above further demonstrates that the ITZ is the weakest part of a concrete matrix. This suggests that the OTZ between substrate-repair concrete will also be demonstrably the weakest link as well. Understanding that the ITZ will exhibit an approximate 50% reduction in strength properties when compared to bulk material will be an important concept when evaluating the results between plain substrate and substrate-repair mixes detailed in this thesis.

It is important to note that the optimum level of substrate moisture condition will be contingent on the properties being evaluated. As noted above, the dry substrate condition has produced an increase in overall shear bond strength when compared to pre-wetted substrates. However, additional studies have shown that when performing pull-off testing, the pre-wetted substrates demonstrated higher strength characteristics and better adhesion than dry substrates [10]. In a collaborative laboratory effort between the Federal Highway Administration (FHWA) and the National Institute of Standards and Technology (NIST), researchers evaluated the shear and pull-off strength between substrate-repair concrete utilizing different moisture conditions and overlay repair material. To evaluate these parameters, researchers utilized two moisture conditions: dry substrate and saturated surface dry (SSD) substrate. The SSD substrate was soaked 24 hours prior to the application of repair material to obtain the desired moisture

condition. The results of the shear strength testing in this study agree with the other published literature reviewed in this thesis—that higher shear strength values are exhibited by the dry substrates when compared to SSD substrates. However, the results of the pull-off testing indicate greater strength and better adhesion for specimens that are pre-wetted. In *Figure 11,* a visual inspection can be performed to witness the level of increased adhesion between the substrate and repair material for the substrates in the SSD moisture condition. The specimens on the left in the image were the SSD substrates and the right side displays the dry substrate specimens. The bright white witnessed in the SSD specimens is repair material that has adhered to the substrate. The increase in adhered concrete for the SSD specimens directly indicates the increase in adhesion due to the substrate moisture condition.

Figure 11: SSD (Left), Dry (Right) Test Specimens. Bright White is Adhered Concrete [10]

The authors conclude that the increase in adhesion for the SSD specimens is most likely attributable to the increase in water availability in the OTZ, therefore increasing the level of hydration of the repair material. They also note that substrate moisture condition is only one parameter affecting the bond strength between substrate and repair material. Repair material fluidity, substrate surface roughness, and substrate moisture condition all play an important role in microstructure development in the OTZ between substrate-repair concrete.

Supplemental research has concluded similar results to the observations published by the FHWA and NIST collaborative effort. Courard et al. also evaluated the impact of substrate moisture condition on adhesion between substrate and repair concretes [11]. In their research, concrete slabs were prepared and conditioned with saturation levels ranging from 40-100%. The saturation levels were determined by directly measuring the water content of small, drilled samples stored at the desired saturation levels. Like the FHWA and NIST research, the authors evaluated the adhesion between substrate and repair specimens by means of pull-off testing. The results of their tests are displayed below in *Figure 12*:

Adhesion of mortar A on concrete substrate versus saturation level of concrete substrate and slurry.

Adhesion (N/mm^2)		
Saturation level	With dry slurry	With wet slurry
50	0.83	2.32
52	2.80	2.14
55	2.09	2.89
70	2.75	2.65
90	3.54	3.36
93	2.13	3.06
97	1.81	2.58
100	1.43	1.48

Adhesion of mortar B on concrete substrate versus saturation level of concrete substrate and slurry.

Adhesion (N/mm^2)		
Saturation level	With dry slurry	With wet slurry
50	1.41	1.34
60	2.90	2.72
70	2.95	1.41
100	1.09	1.43

Figure 12: Adhesion of Mortar. Mortar A (Top), Mortar B (Bottom) [11]

The results of the test indicate low adhesion for substrates prepared with a saturation level less than 50%. They also indicate an increase in the level of adhesion for substrates conditioned to saturation levels between 55-75%. Finally, there was a decrease in adhesion as the level of saturation increased to over 90%. This research has determined a few key findings:

1. Low saturation levels produce weak, or reduced adhesion.
2. Optimum adhesion was achieved for substrates saturated to levels between 55-75%.

3. There remains a wide variation of saturation levels that will generate adequate adhesion, suggesting that slight variations in moisture condition will not negatively affect adhesion.

In agreement with previous published literature, the authors of this study attribute the increased adhesion at saturation levels between 55-75% to the water absorption of the substrate material, increasing mechanical interlock between the substrate and repair materials.

2.2 Transmission X-ray Microscopy

An important consideration when formulating a concrete mix design is the ability of the mix to withstand chloride ion penetration. The intrusion of chloride ions initiates an electrochemical process with the steel reinforcement, creating various degradation mechanisms [12]:

- Expansion: the electrochemical process creates a volumetric expansion of the steel, inducing cracks throughout the concrete.
- Brittleness: corrosion reduces the ductility of reinforcement, leading to increased brittleness.
- Structural capacity: corrosion decreases the cross-sectional area of the steel reinforcement, therefore reducing the structural capacity of the affected element.

The intrusion of chloride ions and resulting corrosion has deteriorated a significant amount of infrastructure in the United States. One study estimated that the cost of corrosion in the U.S. was $137.9 billion [13]. The report further divided the costs into categories and determined the total costs for transportation and infrastructure to be $22.6 billion and $29.7 billion, respectively. The proportion of the costs attributed to bridges alone was $8.3 billion. The state of the Nation's deteriorating bridges, and other infrastructure has been a highlight of multiple industries in the last few decades. The American Society of Civil Engineers (ASCE) has been developing their report card since 1988, where the professional organization evaluates and grades the state of American infrastructure. In their most recent report card, ASCE has rated the bridges in America a "C" due to an estimated 231,000 bridges in need of repair and preservation [14]. Corrosion has a debilitating effect on concrete and American infrastructure.

As a result, techniques and methodologies are needed to evaluate the potential for corrosion in concrete structures.

In steel reinforced concrete elements, the reinforcement remains protected due to passivation. The pH of concrete is generally greater than 12.5 [12]. The high alkalinity of the material creates a layer of protection around the rebar. Additionally, the concrete cover will provide more protection for the steel. However, when enough chloride ions—technically named the chloride threshold level—have diffused through the material, they begin to attack the passivated layer surrounding the reinforcement. Once the passivated layer has dissolved into pore solution, the steel reinforcement remains exposed and corrosion degradation can occur.

The intrusion of ions into the concrete can be transported by different transport mechanisms. A brief description of these mechanisms is provided below [12]:

- Permeation – movement of ions due to pressure gradient.
- Diffusion – movement of ions due to a concentration gradient.
- Migration – movement of ions due to an applied electrical field.
- Absorption – movement of ions due to capillary suction.

Regarding chloride ions and corrosion, the most common transportation mechanism is diffusion. These chloride ions are usually supplied through deicing salts (for regions in cold climates where salt is applied to roadways) or saltwater surrounding the structure. Once the ions are in contact with the structure, they begin to diffuse through the elements due to a concentration gradient. The rate at which these ions can move through a structure can be described by the materials diffusion coefficient (D_C). Currently, there are several published test methods developed to predict the rate at which ions will move through a concrete mix, but only one standard has been accepted to quantify a diffusion coefficient. An overview and description of these test methods is provided below:

- AASHTO T 358 – This test method correlates the electrical resistivity of the concrete to the overall chloride penetration risk. The method requires the use of a Wenner probe to apply a

current on the surface of an element. The measured resistivity is then related to the ion penetration risk. The difficulty in reliability of this test method is the wide variation of results produced between concrete of different saturation levels. It has been demonstrated that dry concrete produces a much higher resistance than wet concrete, challenging the effectiveness of the method [16]. Additionally, the measured resistance received during this test method has depth limitations. The results would generally only indicate surficial penetration risk since the electrical field is not applied throughout the entire depth of the element. And since surface and bulk penetration potential may vary widely, the measured resistance may not provide a holistic evaluation of the structure. Another concern with this test method is the variation in results even when proper in-situ conditions are achieved. AASHTO T 358 states that the test method can be affected by various concrete properties, including aggregate size, aggregate location, and the location of steel reinforcement. These properties can produce a variation in results such that the coefficient of variation (CV) is 6.3%. Finally, since this test method does not actually evaluate the rate at which chloride ions diffusion through a structure, the results can only be correlated to penetration risk and will not quantify a diffusion coefficient.

- ASTM C1202 – One of the most popular methods to evaluate chloride ion penetration risk is the rapid chloride penetration test (RCPT). This test method requires concrete cylinders to be cut into pucks, approximately 2”x4” and placed into cells for testing. The cells contain sodium chloride (NaCl) and sodium hydroxide (NaOH) solutions placed in reservoirs on either side of the puck. Once the pucks are secured in the cells, an electrical current (60V) is applied, and the system measures the total charge passed through the center of the concrete puck. After conducting the test method, the total charge passed through the specimen is related to its penetration risk: a greater magnitude of charged passed is correlated to a greater risk of chloride ion penetration. The difficulty with this test method is that it does not directly measure diffusion. Since this test method utilizes an applied electrical current, the transport mechanism is predominantly migration,

and since this test method does not yield a diffusion coefficient, it is simply an index test, and the results can only be related to penetration risk.

- ASTM C1556 – This test is the *only* ASTM standardized test method that quantifies a diffusion coefficient. In this method, the concrete is sealed on all sides except the surface so that diffusion can be controlled to one direction. After sealing, the specimens are exposed to a sodium chloride (NaCl) solution. Finally, the specimens are ground in layers and the chloride content at each layer is determined. These values are fitted to *Equation 1* and a diffusion coefficient can be calculated.

$$C_{(x,t)} = C_s(1 - \text{erf}\,(\frac{x}{2\sqrt{D_{ac}t}}) \quad (1)$$

Where: C_s is surface iodide concentration; $C_{(x,t)}$ is iodide concentration at a specific depth and time; x is the distance from the surface; t is time; and erf is the error function.

This method allows the researcher to measure not only the depth of penetration, but the concentration at each layer. The main difficulty with this test method is that it is destructive in nature.

- NT Build 492 – This test method is very similar to the ASTM C1202 procedure. The concrete pucks in this method are also placed in cells between NaCl and NaOH solutions with an applied electrical current (30V). After the test is complete, the pucks are split in half and sprayed with a silver nitrate (AgNO) solution. The silver nitrate precipitates where the chloride ions have penetrated, and the depth of penetration can be determined. From there, additional calculations can be made to derive a migration coefficient. The limitations of this test method are the same as ASTM C1202 in that this method is measuring migration, instead of directly evaluating diffusion.

Since the test methods discussed above are either destructive in nature or correlate another transport property to diffusion, alternative test methods are desired. In recent years the use of X-ray microscopy has been employed to image cementitious materials [20-22]. The images received are

analyzed and a diffusion coefficient is derived. A diffusion coefficient is derived like the test method outlined in ASTM C1556. However, in X-ray microscopy potassium iodide (KI) is used as the tracer agent due to its high electron density. This density will allow the solution to absorb a greater number of X-rays, generating a clearer radiograph. The specimens will be ponded with a 0.6 mol/L KI solution for the desired analysis period (7-, 14-, 28-days). Throughout the ponding period, the samples will be removed and scanned in the X-ray scanner. The radiographs will have varying gray values associated with the number of X-rays absorbed. The results of these radiographs will be fitted to the equation displayed in *Equation 1* and will allow the derivation of an apparent diffusion coefficient.

One of the first published studies to incorporate XCT was conducted by Moradllo et al. [23]. In this study researchers performed transmission X-ray microscopy (TXM) and utilized X-ray computed tomography to nondestructively track diffusion in cement pastes. They mixed paste samples with three w/c ratios (0.35, 0.40, and 0.45). After making the samples, they were sealed with a hydrophobic wax and ponded with the KI solution. Following the experiment, the authors were able to address three key components of this test method:

1. The ability of XCT to track ion diffusion.
2. Agreement of XCT derived D_c with other methods.
3. Ability of KI to accurately model chloride ion (Cl^-) diffusion.

The samples in this study were scanned at intervals of 5 hours, 7-, 10-, and 28-days. After scanning, the background image was removed so that the depth of KI diffusion can be viewed. *Figure 13* displays the results of the obtained radiographs. The dark gray emanating from the top of the specimen is KI diffusing down the sample. From the image it can be viewed that as the ponding time increased, the depth of KI solution increased.

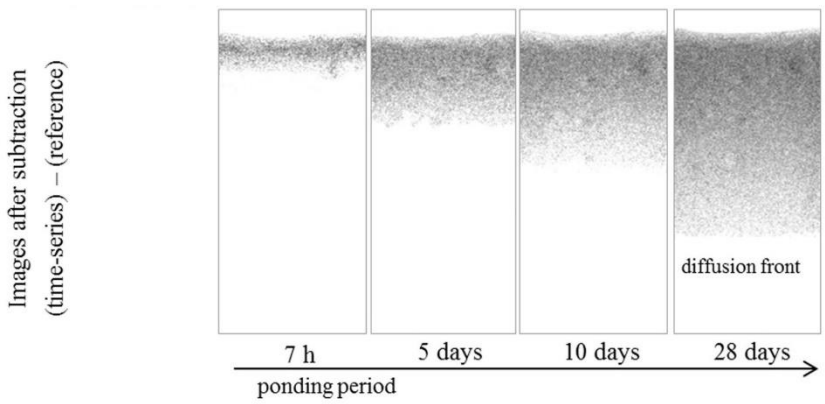

Figure 13: Time-Series Radiographs [23]

The radiographs in the figure demonstrate the ability of XCT to track KI diffusion in the paste samples. To validate the results and accuracy of these radiographs, the specimens were polished and prepared for μX-ray fluorescence (μXRF) analysis. After completing μXRF and performing the analysis, the results were graphed and compared with the TXM results. The outcome of this comparison is displayed in *Figure* 14.

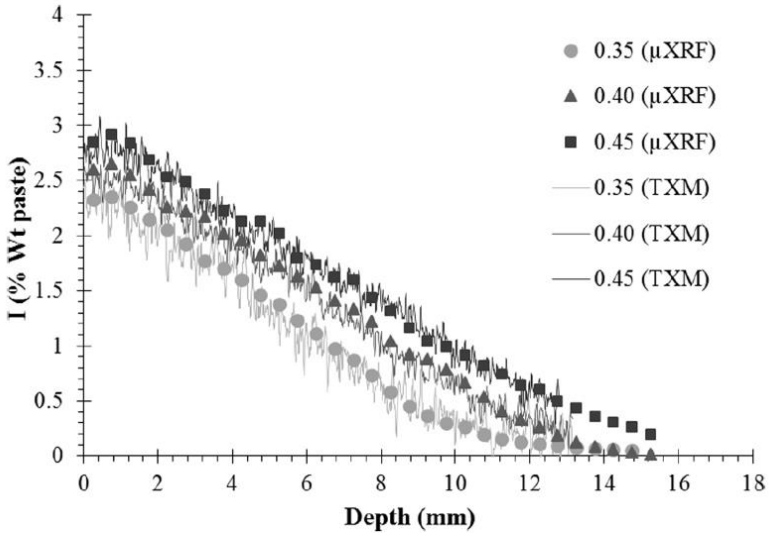

Figure 14: XRF and TXM I Concentration Comparison [23]

The graph demonstrates how accurate the TXM results were when compared to XRF. The authors note that TXM produced diffusion coefficients that were about 8% higher than XRF. Given these results, the authors conclude TXM was able to accurately track iodide diffusion. The final component of the study

was to compare the diffusion coefficients of samples ponded with KI and Cl^-. Since KI was utilized due to its high electron density, its ability to accurately model Cl^- diffusion needed to be verified. The result of this comparison is presented in *Figure 15*.

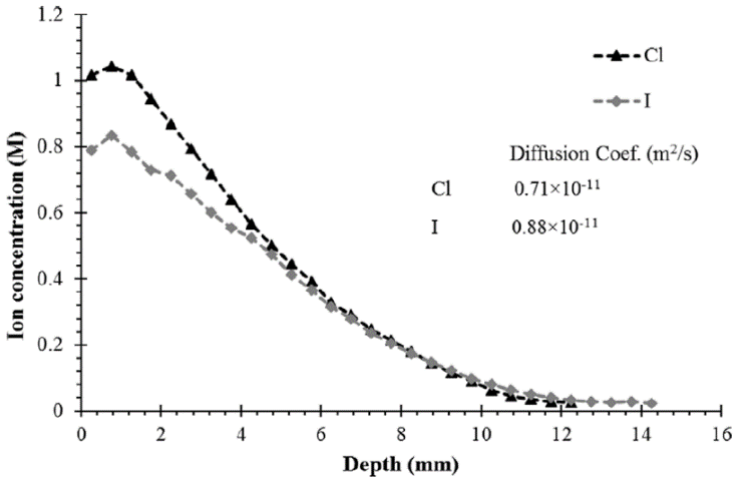

Figure 15: Comparison of I and KI Diffusion Coefficients [23]

After analyzing the comparison, the authors were able to conclude that KI produced diffusion coefficients approximately 24% higher than Cl^-, but still maintained similar concentration profiles. With the obtained radiographs, comparison to XRF, and verification of derived diffusion coefficients, this study was able to solidify TXM as an acceptable, non-destructive, method of tracking diffusion in cementitious materials.

` To expand on the efforts of the Moradllo study, Kang et al. utilized TXM to evaluate the effects of fly ash (FA) and their replacement percentages on the diffusion coefficient of cement paste [24]. The Kang study utilized ASTM C150 Type I Cement and 19 different types of fly ash for their research. To evaluate the effects of replacement percentages, replacements of 20% and 40% FA were incorporated in the samples. The specimens were prepared and ponded with a 0.6 mol/L KI solution. A radiograph was obtained for the samples at 45-, 90- and 135-days. After obtaining the radiographs, the authors utilized *Eq. 1* to derive diffusion coefficients for all the samples. The results of their experiments are presented in *Figures 16 and 17.*

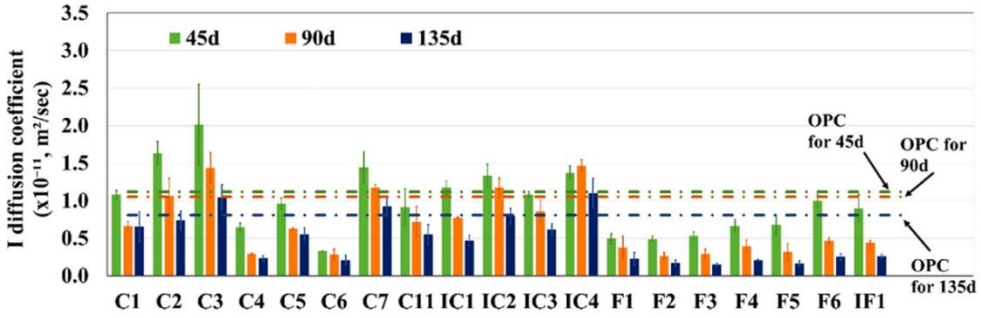

Figure 16: Diffusion Coefficients at 20% FA Replacement [24]

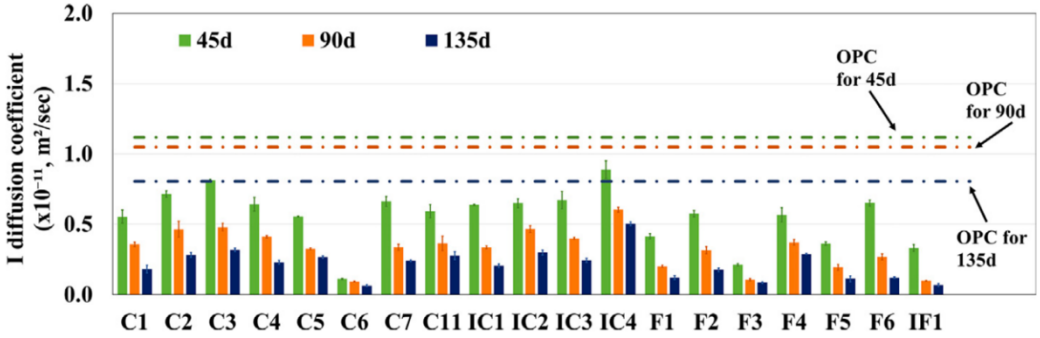

Figure 17: Diffusion Coefficients at 40% FA Replacement [24]

The results of the study indicate that for a replacement of 20% FA, the diffusion coefficient increased when compared to the ordinary portland cement (OPC) control group. An increase in diffusion coefficient would suggest a decrease in durability of the mix. For the 40% FA replacement, the results portray an overall reduction in diffusion coefficient when compared to the control group. This would suggest an increase in durability and improvement in the mix design. When comparing the results of the two replacement percentages, a replacement interval of at least 40% would appear to be optimum. Additionally, for all samples there is a decline in diffusion coefficients as the mix ages. Fly ash hydrates slowly, meaning that as the mixture ages, hydration will continue and increase densification in the microstructure. This continued hydration will result in lower permeability and diffusion coefficients.

In a more recent study, Behravan et al. utilized TXM to evaluate the effects of alternative cementitious materials (ACM). This study evaluated the rate of penetration of five cementitious binders:

- Ordinary portland cement (OPC) – water-to-binder ratio (0.40)
- Calcium aluminate cement (CAC3) – water-to-binder ratio (0.40)
- Calcium sulfoaluminate belite cement (CSA2) – water-to-binder ratio (0.40)
- Calcium sulfoaluminate belite cement with polymer (CSA2B) – water-to-binder ratio (0.40)
- Alkali-activated binder with Class C fly ash (AA1) – water-to-binder ratio (0.21)

The preparation of materials in this study is like the studies conducted by Moradllo and Kang, where samples are created, cured, and ponded with a 0.6 mol/L KI solution prior to obtaining radiographs. Samples in this study were ponded for a total of 28-days, with scans occurring at 5 minutes, 1-, 3-, 7-, 10-, 14-, and 28-days. Prior to obtaining ponded scans, a radiograph was also obtained with no specimen in the scanner. This is utilized as a reference radiograph where background attenuation can be subtracted from the radiographs taken during ponding. To better understand the effects of the different ACMs on porosity, the authors also conducted a modified ASTM C642 to measure the volume of permeable pore space. When evaluating the porosity of a material, it is more important to understand pore connectivity than total porosity since pore connectivity plays a greater role in overall porosity of the concrete matrix. After ponding and obtaining radiographs, the authors were able to derive diffusion coefficients and depth of penetration for all associates mixes. The results of these values are displayed in *Figures 18 and 19*.

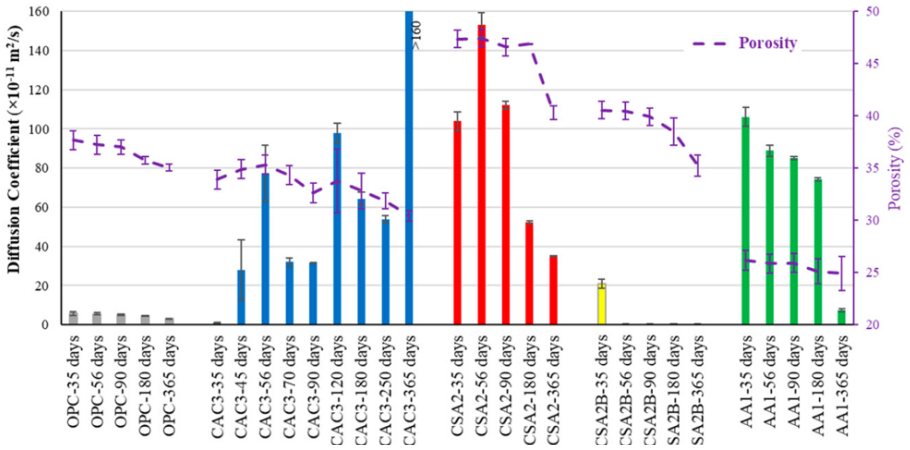

Figure 18: Diffusion Coefficients and Porosity (%) [22]

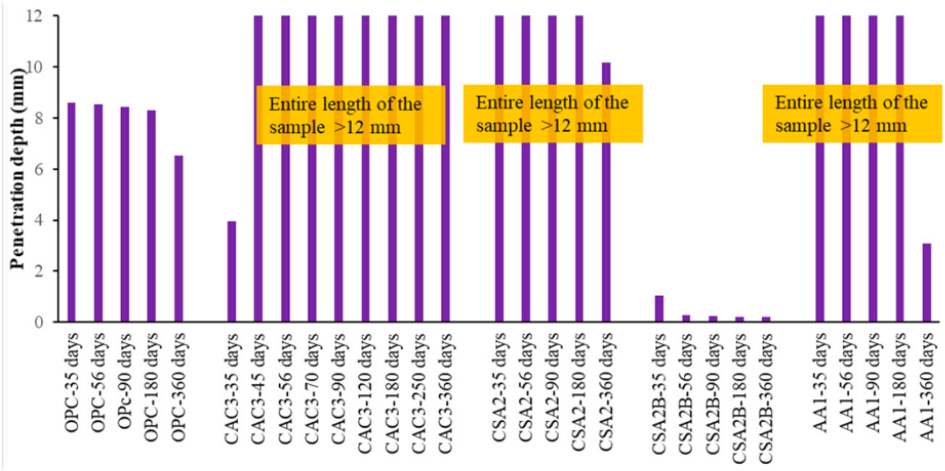

Figure 19: Depth of Penetration [22]

The figures above demonstrate that for the CAC3 binder there was an overall increase in diffusion coefficient as the material continued to age. The other ACMs—CSA2, CSA2B, and AA1—demonstrated an overall reduction in diffusion coefficients the longer the samples aged. It is also important to note the CSA2B binder was the only ACM to demonstrate an improvement in diffusion coefficient when compared to OPC. However, this improvement was not initially realized and required at least 35-days of curing time for the mix to obtain sufficient hydration. This result suggests CSA2B may increase the durability of a concrete mix if given appropriate curing time. The depth of penetration results displays that for three of the ACMs evaluated, the entire specimens were penetrated. This would be of upmost concern for structural elements with steel reinforcement. If the KI was able to penetrate the entire depth of the specimen, it is plausible to believe chloride ions would penetrate the mixture in-situ and degrade the steel reinforcement. As noted with the diffusion coefficient results, the CSA2B binder demonstrated the greatest performance in preventing penetration of the KI solution. This binder outperformed the OPC and maintained the overall lowest depth of penetration of all samples. Another important conclusion from this study is the comparison of porosity to diffusion coefficient. The AA1 binder maintained the lowest total porosity of all binders yet did not demonstrate the lowest diffusion coefficient. This would indicate greater interconnectedness of the pores in the samples and highlight the distinction between pore

interconnectedness and total porosity. Additionally, for this binder there was an overall decrease in diffusion coefficient between 35- and 365-days but little change in the total porosity. The study by Behravan et al. further supplements published literature on the effectiveness of using TXM to evaluate cement and cementitious binders. This study was able to nondestructively evaluate several different binders and compare them to OPC. As researchers continue to search for ACMs due to an increasing decarbonization effort, TXM will be a vital technique in evaluating their effectiveness and appropriate replacement percentages. An overview of the benefits of the technique is outlined below:

- Quick scan time (less than 1 min).
- Minimum sample preparation needed.
- Exceptional repeatability. Diffusion coefficient variation from sample-to-sample was determined to be $\pm 0.16 \times 10^{-11}$ [23].
- Potassium iodide displays strong correlation to chloride ion diffusion and produces similar diffusion coefficients [23].

Despite the numerous benefits of the TXM technique challenges remain:

- Requires the development of calibration curves for each mix design.
- Samples must be oriented the same direction for each scan to accurately track diffusion front.
- Gray values obtained over the face of the samples represent an average over a set region.
- µCT scanners are extremely expensive and may be cost prohibitive.

Since µCT scanners are expensive—approximately $300-$400k for a new scanner—additional techniques are desired. In a National Highway Cooperative Research Program (NHCRP) IDEA Project, a novel concept was introduced to utilize dental X-ray equipment to perform the TXM technique [25]. The project was termed the checking ion potential (CHIP) and works like TXM where radiographs are obtained and analyzed to develop diffusion coefficients. However, in this method the X-ray source is a dental X-ray. From there, the authors utilized commercially available parts to construct a wooden box to

house the sample, X-ray source, sensor, and other necessary components to ensure safe operation. The CHIP system works in the same manner as TXM. Samples will be made with known concentrations of KI and scanned to develop a calibration curve. After the development of the calibration, test specimens can be created, cured, and ponded with the 0.6 mol/L KI solution. These radiographs can be utilized with *Eq. 1* to derive a diffusion coefficient. A schematic of the CHIP system is provided below:

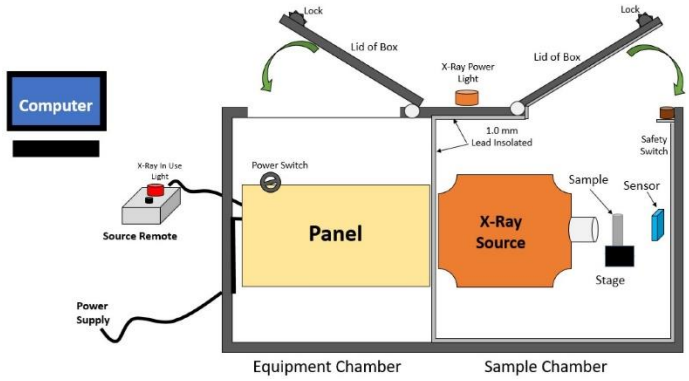

Figure 20: CHIP Schematic [25]

After constructing the CHIP system, the authors were able to obtain radiographs and derive diffusion coefficients for both laboratory and field samples. For the field samples, the researchers retrieved concrete cores and then utilized a mini core to obtain samples from the retrieved field cores. To verify the results of the experiment, the authors also obtained radiographs and analyzed iodide penetration with a µCT. Since the CHIP system is modeled after the µCT scanner, it is important to verify the results of the experiment. The equipment utilized in this experiment is presented in *Figure 21*.

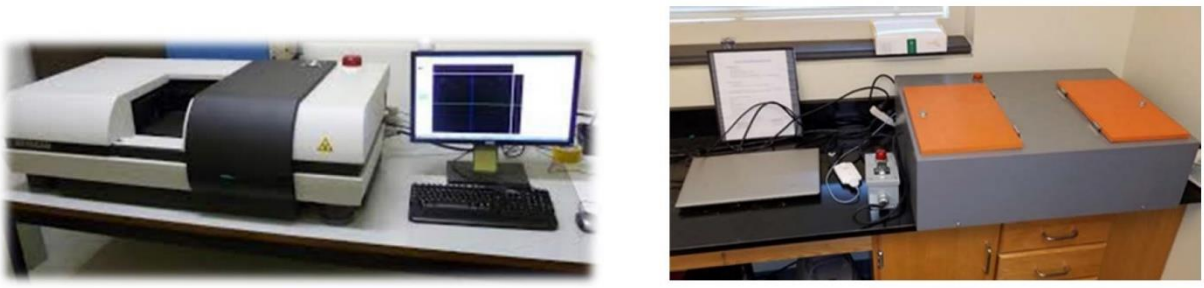

Figure 21: SkyScan 1172 µCT (L), CHIP (R) [25]

After scanning the samples in both machines, the diffusion coefficients were compared. *Figure 22* represents a graph of the derived values:

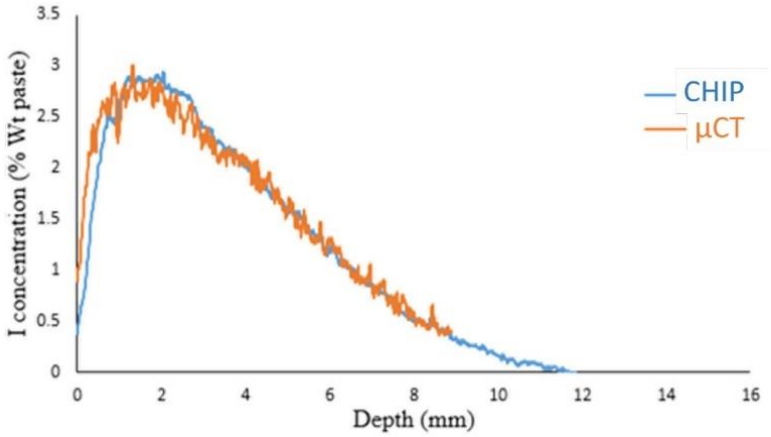

Figure 22: µCT vs CHIP Iodide Concentrations at Depth [25]

The results displayed in the figure display the precision of the CHIP system when compared to a commercial µCT scanner. The major benefits of the CHIP system include availability of parts and costs. Dental X-ray sources can be easily found through third-party retailers for relatively low cost. The sensor can also be purchased online for a competitive price. Overall, the CHIP system will cost approximately $18-$20k depending on the age and condition of the X-ray source. Additionally, the authors of the work discuss how the CHIP system can be modified, making it more durable and field deployable. The ability to nondestructively track diffusion in the field is an advantage of CHIP that is simply not possible for µCT scanners. Besides demonstrating the CHIP system as an accurate method of tracking ion diffusion, the authors were able to evaluate effectiveness of silane treatments on concrete bridge decking. This research was coordinated with Oklahoma Department of Transportation (ODOT) to evaluate 14 different silane sealers and their effectiveness on permeability in bridge decking. Utilizing the TXM procedures outlined thus far in this thesis, researchers were able to evaluate the iodide concentrations at a depth of 2mm for all silane sealers. The results of their efforts are displayed in *Figure 23.*

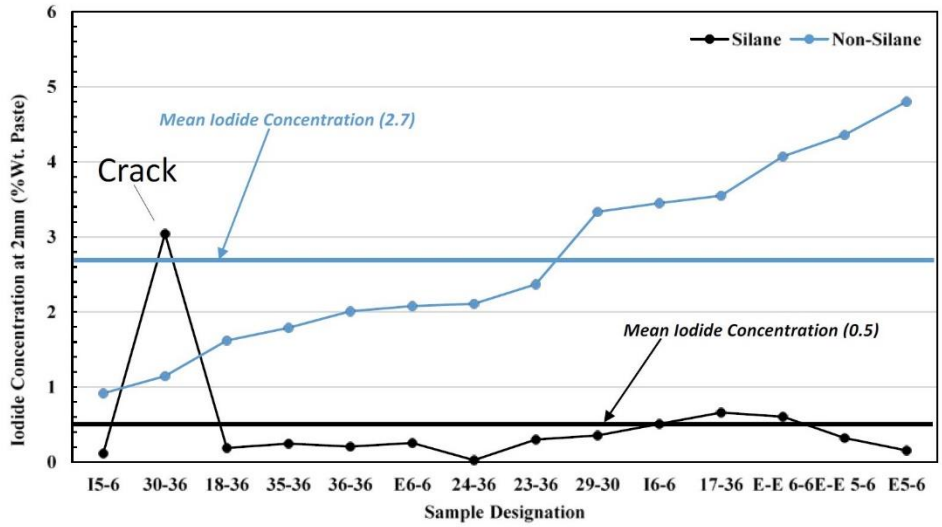

Figure 23: Silane Sealer vs. Iodide Concentration [25]

These results display a significant decrease in mean iodide concentration for the samples with applied silane sealers. The authors note that for sealer designated as 30-36, there was a crack in the sample, generating the outlier in the graph. The ability to evaluate the effectiveness of these silane sealers is yet another benefit of the TXM technique. To date, TXM has been able to track ion diffusion and investigate components such as silane sealers, alternative cementitious materials (ACM), supplementary cementitious materials (SCM), cement pastes and mortars, concrete laboratory samples, and concrete field samples. Given the effectiveness and affordability of CHIP systems, research laboratories would benefit from incorporating this novel idea into their facilities.

2.3 Freeze/Thaw Conditions on Substrate-Repair Concrete

As discussed in the substrate-repair literature review section of this thesis, there are many deterioration mechanisms affecting the serviceability of concrete. One of the most common deterioration mechanisms is freeze/thaw (FT) cycling. As concrete is subjected to cycles of freezing and thawing, damage accumulates as water expands by 9% when it freezes. Through repeated FT cycles, cracks propagate and will eventually lead to spalling of the concrete. This spalling will increase water absorption and exasperate the effects of freezing and thawing. Oftentimes, this is of major concern for concrete elements that have steel reinforcement since exposure of the steel to the ambient environment promotes

corrosion. There are several theories as to why FT damage occurs. A brief description of these theories is provided below [26]:

1. Hydraulic pressure – forcing water out of the pores as water freezes.
2. Osmotic pressure – increase in alkali concentration due to ice formation.
3. Expansion – expansion (by 9%) of water as it freezes.
4. Crystallization pressure – migration of water due to a vapor pressure gradient.
5. Glue spall – difference in linear expansion coefficients between water and cement.

There are additional theories explaining FT damage that are not contained within the list above. Wang et al. provides a comprehensive review on the various theories surrounding freeze/thaw damage and their accompanying research [26].

The damage associated with FT cycles is well known and evaluated throughout literature. A schematic of the damage induced by FT cycles is provided below. As water fills the voids and begins to freeze, cracks are generated within the microstructure, leading to scaling.

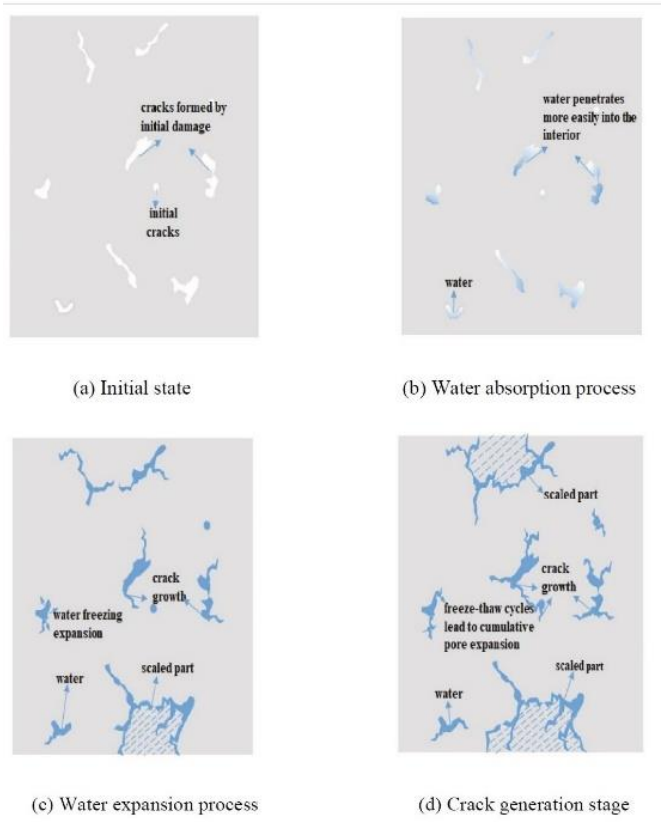

Figure 24: Freeze/Thaw Crack Propagation [26]

The most common method of evaluating internal damage associated with FT cycles is the measuring of relative dynamic modulus of elasticity (RDME) in relationship to the number of freeze/thaw cycles. Research has shown that as the number of FT cycles increases, the RDME dramatically decreases, with an increase in water absorption. One study evaluated RDME and water absorption incorporating various freezing and thawing cycles [27]. These cycles include, standard test cycle (STC), long freezing duration (LFD), slow freezing rate (SFR), and rapid freezing rate (RFR). A graph representing these findings is presented in *Figure 25*.

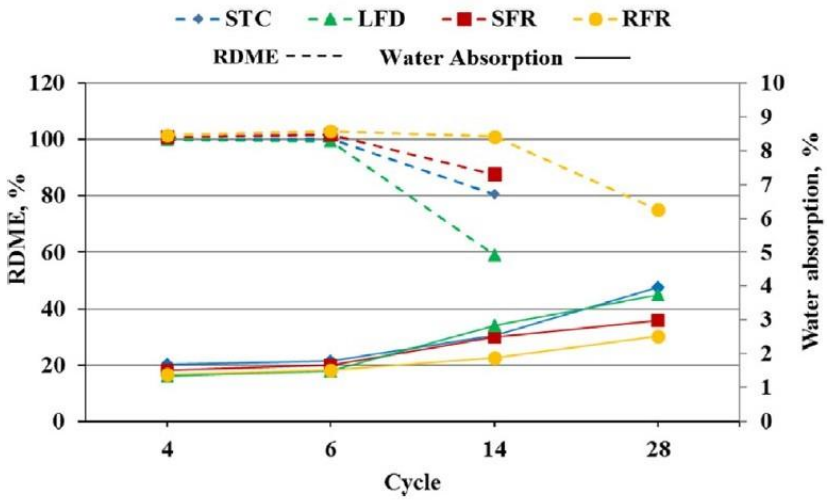

Figure 25: FT Cycle vs. Water Absorption and RDME [27]

The graph above demonstrates that following the sixth FT cycle, there is a dramatic reduction in RDME and an increase in water absorption. These results are due to the microstructure changes occurring due to repeated freezing and thawing. These changes include an increase in pore volume, pore surface area, pore interconnectivity, and an increase in crack propagation. The relationship between pores and FT cycles has been evaluated through microstructure evaluation [28]. Researchers have been able to quantify this relationship and the results of their findings is presented below in *Figure 26*.

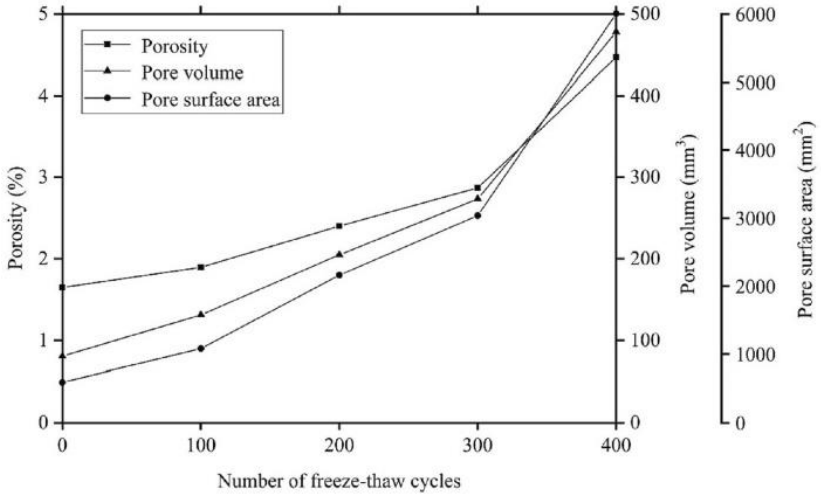

Fig. 8. Evolution of internal pore structure of hydraulic concrete under FT action.

Figure 26: FT Cycles vs. Porosity, Surface Area, and Volume [28]

The authors of this study were also able to conclude that during FT cycles cracks and pores originally in the concrete were connected and expanded during the FT cycles. This connection of cracks and pores increased the pore interconnectivity and had a much greater effect on porosity than the total number of pores in a concrete matrix.

An important area of research for this thesis is the effect of FT cycles on the ITZ. This thesis will contain research aimed at understanding the impact of substrate moisture condition between the substrate-repair concrete and what impact this has on strength and FT resistance of the bond. As a result, the effect of FT on the ITZ will directly correlate with the effect on the OTZ of substrate-repair concrete. As discussed in the substrate-repair literature review, the ITZ—and ultimately the OTZ—are considered the weakest part of the concrete matrix. This region has been known to contain a decreased cement paste content, increased porosity, and improper gradation with an increase in smaller particles near the interface. One study was able to identify an increase in porosity along the ITZ that was associated with damage induced by FT cycles. This damage led to an overall increase in porosity along the ITZ of 52% after 400 FT cycles [28]. By utilizing U-net segmentation, the authors were able to model the increase in

porosity along the ITZ. The result of their model is in *Figure 27* and demonstrates the significant increase in porosity as a function of FT cycles.

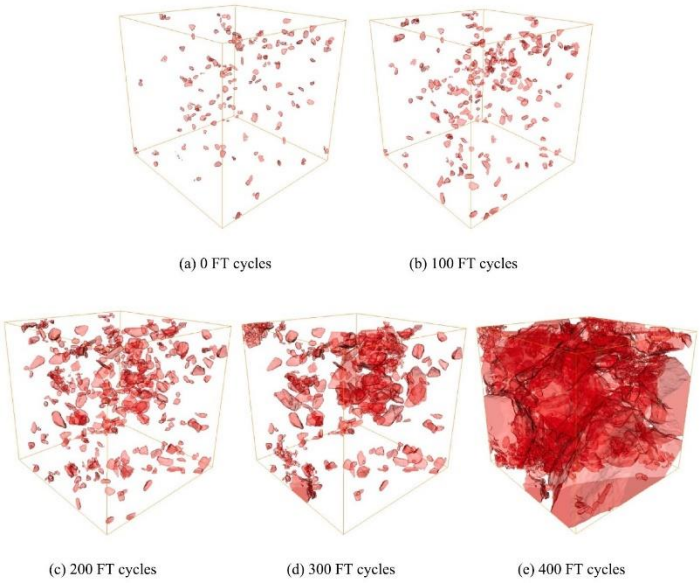

Figure 27: Pore and Crack Evolution in ITZ [28]

The authors also determined the increase porosity in the ITZ is due to the connectivity of cracks and pores because of the FT cycles. The initial cracks and pores in the microstructure were connected during the rapid freezing and thawing, generating an increase in the porosity. The deterioration of the ITZ because of FT cycles has also been evaluated in additional research. In a study evaluating FT effects on concrete pavements, researchers determined that crack propagation ran along the ITZ, increasing the width and size of this transition zone [29]. They were able to determine that micro-hardness significantly decreased with increasing FT cycles and the width of the ITZ grew at a rate of 2.5 times faster than the control group.

Since the specimens in this research were prepared to evaluate the OTZ of substrate-repair concrete, published literature surrounding the effects of FT cycles on the OTZ is vital. One particular study evaluated FT damage of new-to-old concrete utilizing two separate surface preparations: roughened and smooth [30]. The authors were able to determine that FT damage generally occurs in two phases: an initial, accelerated damage phase and a secondary phase where FT damage progresses more slowly. This

is in comparison with substrate concrete which tends to experience FT damage more gradually. The researchers attribute the initial, accelerated damage phase to the weakening of the bond between new and old materials. Furthermore, the authors also determined that roughened substrate surfaces significantly improved resistance to FT damage.

Figure 28: FT Damage Rough Surface. 0-Cycles (L), 50-Cycles (R) [30]

Figure 29: FT Damage Smooth Surface. 0-Cycles (L), 50-Cycles (R) [30]

Figures 28 and *29* display the damage associated with increased FT cycles for each substrate surface condition. The smooth substrate surface condition experienced the greatest FT damage, ultimately leading to debonding of the new-to-old material. For the roughened surfaces, the fracture plane did not always initiate through the OTZ, as some fractures were evident through the aggregates across the bond. This would indicate greater bond adhesion between new-to-old concrete with roughened surfaces. The research presented provides an important distinction between the FT damage experienced in substrate concrete and the damage experienced between substrate and overlay material. Additionally, this research demonstrates the importance of surface preparation on bond durability.

Additional research has been conducted to evaluate the strength of concrete subjected to freezing and thawing cycles. One study utilized pressure tension (PT) testing to evaluate the tensile strength of

concrete after subjection to FT cycles. The authors utilized this test method since it was discovered that compressive strength (CS) testing produced unreliable results. This is due to the direction of loading and orientation of microstructure cracks in the concrete. When the specimen is subjected to compression, the pressure acts to compress the cracks and voids within the microstructure. Therefore, this study not only evaluated the tensile strength of concrete after FT, but it also compared these results to the specimens that were tested for compressive strength. They were able to conclude that tensile strength testing (PT testing) was able to identify deterioration as a result of FT much sooner than compressive strength testing [31]. To evaluate the effects of concrete mix design on the strength properties of the specimens, the authors created samples utilizing two w/c ratios, 0.45 and 0.65. Since a higher water to cement ratio contains greater water content, it would be expected to experience degradation at a faster rate than the specimens made with a lower w/c ratio. Additionally, with a decreased w/c ratio, the microstructure of the concrete will be denser and would ultimately contain fewer voids and pores. The results of both compressive strength and pressure tension testing are presented in *Figure 30*.

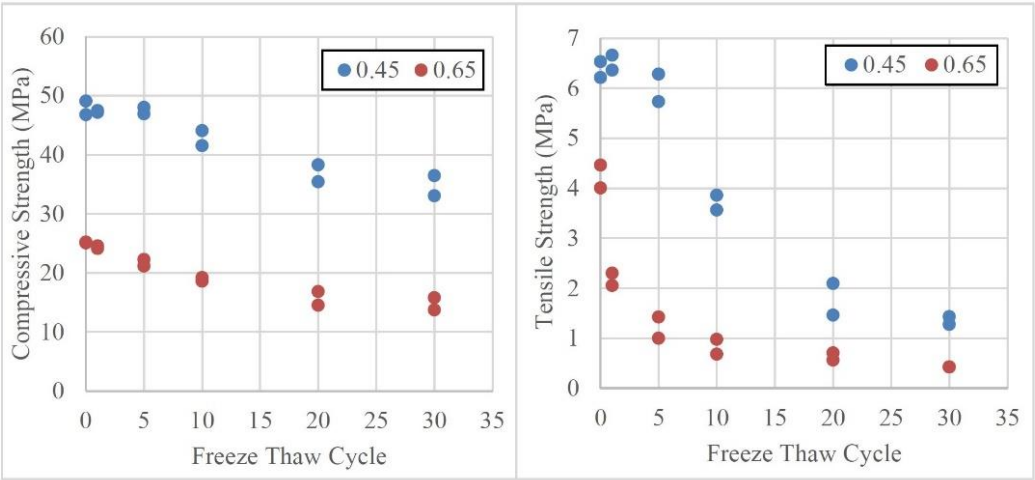

Figure 30: FT Cycles vs. Compressive and Pressure Tension [31]

Utilizing the results of the study the authors were able to identify that after 30 FT cycles, the strength of the 0.45 and 0.65 w/c ratio decreased by 78% and 98%, respectively. Furthermore, the 0.65 w/c ratio decreased in strength more rapidly than the 0.45 w/c ratio specimen. It was determined that after only one cycle the 0.65 specimens demonstrated only 49% of their original strength, where it took a total of 10 cycles for the 0.45 samples to reduce to 42% of its original strength. Also, to compare the results of the compressive and pressure tension tests, the authors combined the results above and this graph is displayed in *Figure 31.*

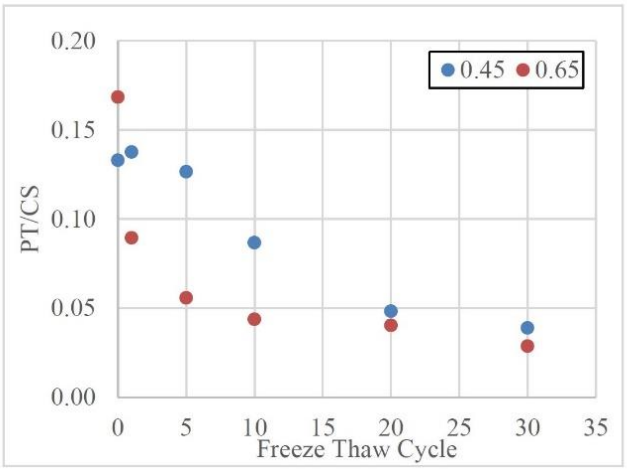

Figure 31: FT Cycle vs. PT/CS Ratio [31]

Since the PT tests were able to identify a reduction in strength sooner, it can be said that this test method is able to identify deterioration because of FT damage sooner than CS testing. Another important finding in this study is the location of the failure plane after pressure testing. The authors noted that after only a few FT cycles, the fracture surface passed through the aggregates. However, after several FT cycles, the failure plane passed around the aggregates. This indicates the failure plane passed through the ITZ and that as FT cycles and damage increases, the ITZ is deteriorating faster than the surrounding concrete matrix

Other research has confirmed the findings of the previous study: a reduction in strength associated with an increase in FT cycles. A study by Sun et al. tested the strength of concrete specimens subjected to FT cycles with varying water-to-cementitious (w/cm) ratios: 0.26, 0.32, 0.38, and 0.45 . After subjecting the specimens to a combination of load and FT cycles under varying stress ratios, they also

determined that concrete with lower w/cm ratios performed better and exhibited greater strength properties. Furthermore, they determined that for the 0.45 w/c ratio, the specimen demonstrated a 45.8% decrease in flexural strength after 20 FT cycles and a stress ratio of 0.5. Additionally, the researchers incorporated air entraining agents (AEA) to evaluate its effectiveness on reducing FT damage. For these specimens they determined the reduction in flexural strength to be only 15% after 500 FT cycles at a stress ratio of 0.5. These results demonstrate the effectiveness of AEA on mitigating FT damage.

Although mitigating freeze/thaw damage is not within the scope of this thesis, it is important to note that there remain several mitigating techniques currently utilized in the industry. As mentioned above, air entraining agents (AEA) are often utilized and are one of the most common chemical admixtures incorporated in a mix design to limit FT damage. Additional techniques employed to mitigate FT damage are the incorporation of supplementary cementitious materials (SCM). These materials provide various mechanical advantages and often create densification of the microstructure. A few of the current SCM's include fly ash, silica fume, rice husk ash, metakaolin, nanoparticles, and the inclusion of hydrophobic materials (both in the mix and applied retroactively) [26]. Wang et al. provides a summary on the current FT damage mitigation techniques and their effectiveness.

3. Section 1: Substrate-Repair Concrete

3.1 Background

To evaluate the optimum substrate surface moisture content on the strength properties of substrate-repair concrete, multiple standardized and unstandardized test methods were performed. These tests include 3-point flexure testing, 4-point flexure testing, RILEM fracture testing, and rapid chloride penetration test (RCPT). Since each test method includes a distinct preparation and testing method, Sections 3.2 and 3.3 will be divided into three separate sections: flexural strength, fracture energy, and RCPT. The discussion of 3- and 4-point flexure tests will be combined in the subsection named flexural strength since the test methods for these specimens are similar.

Prior to the casting of any specimen, a concrete mix design needed to be established. Since the intended application of this research is aimed at concrete repairs and more specifically, bridge decking repairs, a low water-to-cement (w/c) ratio was desired. To better simulate the type of w/c ratio incorporated in bridge structural elements, a w/c ratio of 0.45 was utilized. In selecting proportions for the concrete mix design, the volumetric standard published in the American Concrete Institute (ACI) 211.1-91 was utilized [33]. The mix design is displayed in *Table 1*.

Table 1: Concrete Mix Design for 1yd^3

Component	Volume Fraction	Design (lb/yd^3)
Cement	0.14	744.4
Water	0.20	335.0
Fine Aggregate (SSD)	0.33	1561.0
Coarse Aggregate (SSD)	0.30	1305.1
Air	0.03	-

There remain several commercially available repair mixes for degraded concrete sections, including asphalt overlays, polymer modified concrete overlays, latex modified concrete (LMC) overlays, and portland cement concrete overlays [34]. Concrete overlays are further separated into bonded and unbonded overlays [35]. Although each overlay alternative has a successful project history, the research presented in this thesis utilized a portland cement concrete mix as the bonded repair material when casting

the substrate-repair concrete specimens. Furthermore, both the substrate and repair mix designs utilized the proportions established in *Table 1*.

The cement utilized in the concrete mix design was a commercially available Type I/II portland cement. This is a general-purpose cement and may not be typical of the high early strength (Type III) necessary for rapid bridge decking or concrete pavement repairs. To increase the workability of the concrete mix, a commercially available high range water reducer (HRWR) was incorporated into the mixing water of each batch. An iterative process was utilized to determine the adequate amount of HRWR to incorporate into the design. Too little HRWR will generate an overly dry, unworkable mix that will be difficult to properly consolidate and create specimens. However, adding too much HRWR risks segregation, which is a phase separation between cement paste and aggregates. After a few trial batches, a dosage of 1.5 fluid ounces/100 pounds of cementitious was utilized.

When selecting and proportioning the aggregates for a concrete mix design, the aggregates' absorption capacity (AC) and moisture content (MC) are important material properties that need to be considered. In an aggregate, the moisture content refers to the volume of water within the voids. The absorption capacity of an aggregate is the total volume the aggregate will consume before all voids are fully saturated. If an aggregate maintains an MC below the AC, it will absorb some of the mixing water in the design and locally reduce the w/c ratio around the aggregate. Therefore, understanding the volume of water in an aggregate (MC) and the volume of water needed for saturation (AC) is of high importance in ensuring quality of the mix design. Since the aggregates at the Thomas M. Murray Structures and Materials Laboratory are maintained outside, their MC will vary throughout the year. To ensure an accurate mix design and consistent MC, all aggregates utilized for concrete batching were oven dried for approximately 18-24 hours. Since the aggregates were devoid of water, an accurate AC needed to be determined so that the mixing water could be altered to account for the aggregate's absorption. To do this, ASTM C127 and C128 were conducted to derive the AC for both fine and coarse aggregates [36, 37]. The

absorption capacities for both aggregates as well as other important material properties are displayed in *Table* 2.

Table 2: Material Properties

Component	Specific Gravity	Absorption Capacity (%)	Moisture Content (%)	Fineness Modulus
Cement	3.15	-	-	-
Fine Aggregate	2.57	3.6	0	2.6
Coarse Aggregate	2.77	1.4	0	-

Additional parameters to consider when selecting and proportioning a concrete mix design are slump and compressive strength. To determine the slump and compressive strength of the mix, concrete was batched according to ASTM C192 [38]. Once the concrete was adequately mixed, the slump of the mix was determined to be 1" by utilizing ASTM C143 [39]. Finally, after mixing and curing 4"x8" concrete cylinders, ASTM C39 was conducted to determine compressive strength [40]. The 28-day compressive strength of the mix design established in *Table 1* was evaluated to be 4,630 pounds per square inch (psi) with a standard deviation of 134.2 psi.

3.2 Methods and Procedures

As discussed in the Background, Section 3.2 Methods and Procedures will be divided into three separate sections: flexural strength, fracture energy, and rapid chloride penetration test (RCPT). These subsections are created to efficiently detail specimen preparation, test methods, and results since each parameter evaluated utilized a specific standard.

Flexural Strength

To evaluate the flexural strength and the effect of substrate surface moisture condition on substrate-repair concrete, several specimens were created at varying surface moisture conditions. The moisture conditions evaluated in this thesis were saturated surface dry (SSD), sub-saturated surface dry (Sub-SSD) and oven dry (OD). Since the substrate moisture conditions needed to remain consistent throughout all testing procedures performed, the use of an environmental chamber was employed. The Cincinnati Sub Zero ZPH-16-3.5-3.5-SC/AC environmental chamber allowed the specimens to be

conditioned in a controlled environment with regulated temperature and humidity—ensuring accuracy across all desired moisture conditions. To simulate the three desired substrate moisture conditions, the chamber was set to a constant temperature and varying relative humidity (RH) of 98%, 80%, and 10%. The varying RH conditions represent SSD, Sub-SSD, and OD, respectively. A summary of the desired substrate moisture conditions and their chamber settings is provided below:

1. Saturated Surface Dry (SSD) – Temperature: 20°C, Relative Humidity: 98%
2. Sub-Saturated Surface Dry (Sub-SSD) – Temperature: 20°C, Relative Humidity: 80%
3. Oven Dry (OD) – Temperature: 20°C, Relative Humidity: 10%

The substrate material for the specimens used in flexural testing were batched according to ASTM C192 in 3”x3”x12” prism molds [38]. After the substrate was allowed to cure for 35-days, they were sawcut at midspan of the prism. Once cut, the substrate halves were washed and wiped clean to remove any remaining debris. Next, the substrate halves were placed in the environmental chamber at the desired relative humidity for 18 ± 2 hours. After surface conditioning was complete, the substrate halves were removed from the chamber, placed back into the prisms molds where the repair material was cast alongside. This process was completed for each desired moisture condition: SSD, sub-SSD, and OD. *Figure 32* depicts a schematic of the substate-repair specimens:

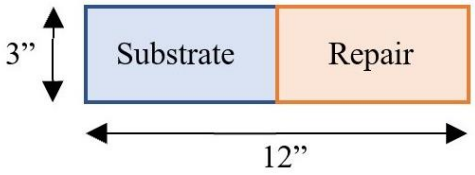

Figure 32: Substrate-Repair Flexural Specimen

It is important to note that adhesion issues developed during the preparation of substrate-repair concrete for the OD (10% RH) substrate moisture condition. During preparation of these samples, the repair material did not adequately bond to the substrate. When attempting to demold the substrate-repair specimen, the repair split away from the substrate directly along the OTZ. *Figure 33* is of the failed

specimen. It can be seen from the photos that there appears to be no adhesion between the substrate and repair material.

Figure 33: Failed Adhesion (10% RH). Substrate (Left), Repair (Right)

We believe there are a few possible reasons for the lack of adhesion between the substrate and repair material:

1. Substrate splitting procedure: sawcut vs. surface abrasion
2. Low substrate moisture condition
3. Increased voids in repair material

Published research reviewed for this thesis has explored the importance of surface preparation when bonding repair material. It was discovered that manually abrading the substrate surface increases the mechanical interlock between the substrate and repair material [10]. In this study the authors observed a decrease in slant shear and pull-off strength when the substrates were bonded with smooth surfaces. The authors explain that during densification of the concrete matrix, the cement particles can pull into and fill voids along the roughened surface. This allows a greater mechanical interlock and thus, increases the adhesion between the two materials. Additionally, the same study demonstrated low adhesion for substrates with dry surfaces. *Figure 11* pictured above in Section 2.1, displays an image from this study displaying the increased adhered concrete for substrates that were conditioned to SSD. Since the substrate-repair concrete specimens utilized for oven dry conditions contained very little surface moisture, this may be an

additional cause of the adhesion failure. Lastly, the increase in voids and porosity along the OTZ, especially for dry substrates, may be attributable to the lack of adhesion experienced in this study. The increased voids can be understood from a visual inspection of *Figure 33* where an increased void content is witnessed in the repair material when compared to substrate. This increase in voids for dry substrates has been reported in other studies to have significantly impacted moisture exchange between the two materials [41]. This increase in voids is due to air voids in the substrate material being forced out as the substrate absorbs water from the repair material. This moisture exchange generates voids along the OTZ and may be the reason for the failed adhesion of our 10% RH flexural specimen.

To test the flexural strength of the substrate-repair concrete specimens, two testing standards were performed: 3-point loading (ASTM C293) and 4-point loading (ASTM C78) [42, 43]. The substrate-repair concrete specimens were allowed to cure for 35-days in a fog room before being removed for testing. The figures below represent schematics of the testing apparatus for each testing standard:

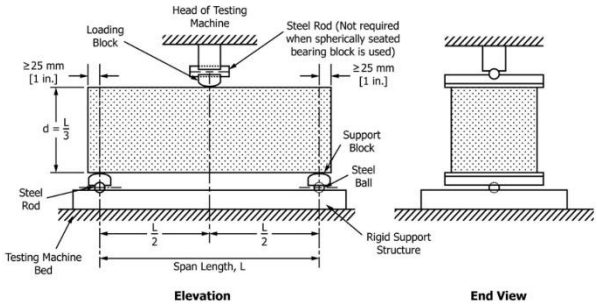

Figure 34: 3-Point Loading. ASTM C293 [42]

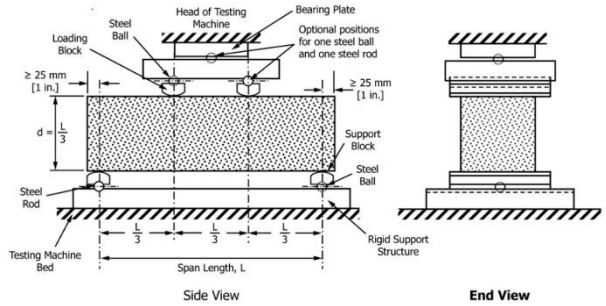

Figure 35: 4-Point Loading. ASTM C78 [43]

Prior to the testing of substrate-repair concrete specimens, pure substrate prisms were tested to identify a baseline for analysis. These substrate specimens were cured the same amount of time as the substrate-repair specimens (70 days). *Figure 36* shows a substrate specimen just prior to performing 3-point loading:

Figure 36: 3-Point Loading on Substrate Specimen

Fracture Energy

To evaluate the fracture energy of the substrate-repair concrete at varying substrate moisture conditions, several concrete prisms, measuring 27.4”x3.4”x6.0” were batched to produce a single-edge notched beam (SENB) fracture geometry. These specimens were created like the specimens utilized to test flexural strength, except for an induced notched on the bottom of the prism. To facilitate crack propagation along the center of the prisms, a small (~3mm thick) piece of sheet metal was placed approximately 1/3 depth between the two halves of the concrete. The insertion of the sheet metal generated a small notch on the bottom of the prisms to prevent adhesion between the halves. This notch is created to follow the testing parameters established in the RILEM draft recommendation for the two-parameter fracture model (TPFM) and serves as the crack initiation point [44]. A schematic of the prisms with the induced notch is presented in *Figure 37*.

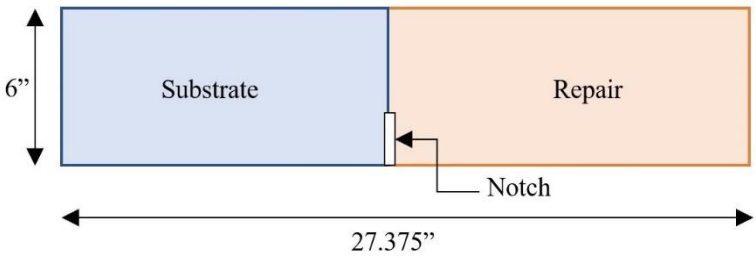

Figure 37: Fracture Prism

All SENB fracture specimens were created with the incorporated notch, including the substrate prisms for use as a baseline. To ensure accurate notch depth, the sheet metal pieces were marked at 2-inches so that all specimens received the same sized notch. A close-up image of the actual notch is displayed in *Figure 38.*

Figure 38: Induced Notch. Substrate (Left), Repair (Right)

The specimen batching for the fracture testing was the same as the flexural strength specimens. That is, the substrate concrete was batched according to the mix design in *Table 1* and allowed to cure in the fog room for 35-days. After the curing period, specimens were removed from the fog room, saw cut in the middle, washed clean of debris, the surfaces were conditioned in the environmental chamber, and the repair material was batched alongside the substrate with the inclusion of a notch. The surfaces were conditioned the same as well, with three substrate moisture conditions being evaluated: SSD (98% RH), Sub-SSD (80% RH), and Oven Dry (10% RH). Again, the specimens were placed in the environmental chamber for 18 ± 2 hours. After the specimens were sufficiently conditioned, repair material was batched

alongside the substrate. These substrate-repair concrete prisms were allowed to cure in the fog room for an additional 35-days after batching the repair material. Following the curing period, the specimens were removed and subjected to the testing procedures outlined in the RILEM draft recommendation. An image of the testing set-up is presented in *Figure 39*.

Figure 39: RILEM TPFM Testing

During fracture testing, a clip gauge was attached on the induced notch, as pictured in *Figure 39*. During the procedure, the crack displacement (crack mouth opening displacement, CMOD) is measured along with the applied load to develop a load vs. CMOD curve. This information will be utilized during the analysis portion of the test to determine the Young's modulus (E), critical effective crack length (a_c), critical stress intensity factor (K^s_{Ic}), critical crack tip opening displacement (CTOD), initial fracture energy (G_{Ic}), and total fracture energy (G_F). An explanation of the derived values is provided below:

- Young's modulus (E): relationship between stress and strain of a linear elastic material.
- Critical effective crack length (a_c): the length a crack must propagate for the specimen to critically fail.
- Critical stress intensity factor (K^s_{Ic}): stress intensity at the critical effective crack length, or the stress necessary to reach the tip of the critical effective crack.
- Critical crack tip opening displacement (CTOD): crack displacement at the top of the critical effective crack.

- Initial fracture energy: the strain energy release rate.
- Total fracture energy: normalization of the total fracture work to the fracture area.

These parameters will characterize the fraction resistance and energy dissipation of the substrate-repair prisms. They will also allow the determination of the maximum load a specimen can resist. The benefit of the TPFM test method is that it allows identification of these parameters from a simple SENB geometry.

Rapid Chloride Penetration Test (RCPT)

A key parameter in evaluating the durability of concrete is its resistance to chloride ion penetration. The research discussed in this thesis surrounds the evaluation of the OTZ of substrate-repair concrete and the effect of substrate moisture condition. As discussed in the literature review of this thesis, the OTZ of substrate-repair concrete is considered the weakest area in a concrete matrix and will experience increased porosity and voids. This will inherently affect the durability of the matrix and its resistance to chloride ion penetration. To study this effect, substrate-repair concrete cylinders (4”x8”) were batched according to ASTM C192 and prepared for testing. Testing for this parameter consisted of performing ASTM C1202, electrical indication of concrete’s ability to resist chloride ion penetration, by using a commercially available RCPT system [17]. These cylinders were batched according to the mix design proposed in *Table 1* and allowed to cure for 35-days. Following the 35-day curing period, cylinders were removed from the fog room and saw cut longitudinally in preparation for substrate moisture conditioning. The cylinder halves were conditioned according to the same substrate conditions previously discussed with flexural and fracture testing: SSD (98% RH), Sub-SSD (80% RH) and Oven Dry (10% RH). The specimens were placed in the environmental chamber for 18 ± 2 hours to ensure substrate moisture condition. After the conditioning period the cylinder halves were removed, and repair material was batched alongside the substrate. A schematic of the cylinders along with dimensions is provided below.

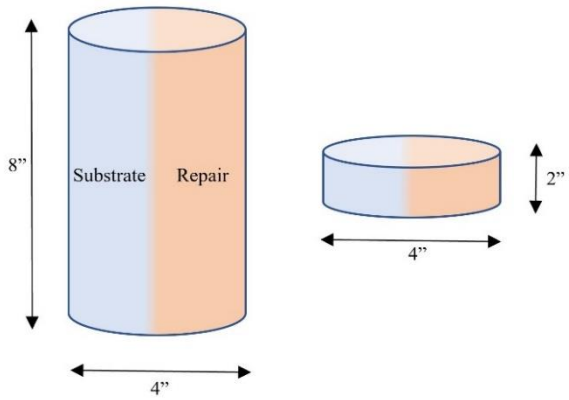

Figure 40: RCPT Cylinder and Puck Schematic

The substrate-repair cylinders were allowed to cure in the fog room for 35-days prior to preparation for RCPT. An example of a substrate-repair cylinder that was cast for the 80% RH (Sub-SSD) testing procedure is also displayed in *Figure 41*.

Figure 41: RCPT Cylinders (80% RH); Substrate (S), Repair (R)

To prepare for RCPT, the cylinders were removed, and both ends were sawcut to ensure even surfaces. Then, the cylinders were cut into approximately 2”x4” pucks (displayed in *Figure 41*). After cutting the pucks, a commercially available two-part epoxy was applied to the outside of the pucks. The epoxy provides a barrier around the outside of the puck, preventing chloride migration from occurring

through this area. This allows for a more accurate determination of chloride ion penetration risk. Once the pucks are sufficiently sealed and the epoxy is set, they needed to be conditioned prior to testing. ASTM C1202 provides instructions on the required conditioning. First, the pucks are placed in a vacuum chamber for a few hours and then submerged for several hours thereafter. The total time required for conditioning (vacuuming and submersion) is 22 ± 2 hours. Utilizing a commercially available RCPT system, the pucks are placed in cells filled with two solutions: 3.0% sodium chloride (NaCl) and 0.3 M sodium hydroxide (NaOH). An electrical potential (60V) is applied, and a charge is forced through the concrete pucks. At the end of testing, the total charge passed through the puck is related to the concrete's chloride ion penetration risk, where the greater charge passed through, the higher the risk of ion penetration. Since the test method for RCPT is utilizing a difference in potential to transport the ions, migration is the transport mechanism being measured. However, published literature has demonstrated strong correlation between electrical resistivity and chloride ion diffusion [45]. Therefore, the analogous test results can be applied to evaluate a specimen's risk for chloride ion penetration. *Figures 42 and 43* display the vacuum chamber used for puck conditioning and the RCPT system that was used in this research.

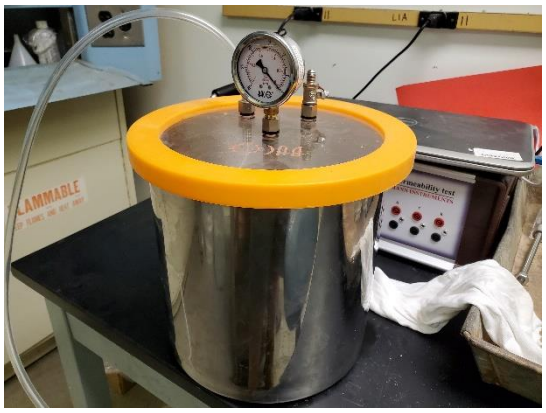

Figure 42: RCPT Vacuum Chamber

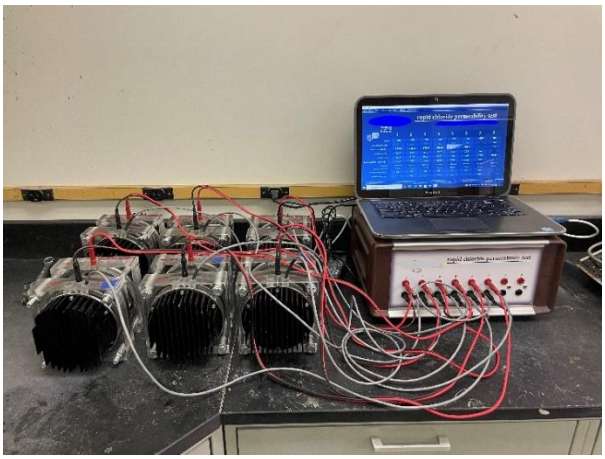

Figure 43: RCPT System

3.3 Results and Discussion

Flexural Strength Results and Discussion

The results of flexural strength testing are presented in *Tables 3, 4, 5, and 6.* All substrates were cured 35-days prior to casting repair material. The substrate-concrete specimen was cured for an additional 35-days. None of the specimens required any capping or shimming. *Table 3* shows the results from 3-point flexural testing, and *Table 4* displays a comparison of the averages from each substrate moisture condition tested:

Table 3: 3-Point Flexural Testing Results

Specimen	Test	Max Load (lbf)	Span Length (in)	Specimen Depth (in)	Specimen Width (in)	Modulus of Rupture (psi)
Substrate	1	2005.5	9.25	3.00	3.10	995
	2	2106.9	9.25	3.00	3.15	1035
	3	1879.7	9.25	3.01	3.10	930
	Average	**1997.4**	-	-	-	**985**
	Std. Dev.	-	-	-	-	**50**
98% RH	1	770.2	9.25	3.10	3.00	375
	2	736.7	9.25	3.10	3.00	360
	3	572.9	9.25	3.05	3.10	280
	Average	**693.2**	-	-	-	**340**
	Std. Dev.	-	-	-	-	**50**
80% RH	1	503.2	9.25	3.05	3.20	235
	2	1115.6	9.25	3.05	3.10	535
	3	1090.1	9.25	3.00	3.15	520
	Average	**903.2**	-	-	-	**430**
	Std. Dev.	-	-	-	-	**170**
10% RH	1	935.4	9.25	3.05	3.15	440
	2	1197.6	9.25	3.05	3.20	560
	Average	**1066.5**	-	-	-	**500**
	Std. Dev.	-	-	-	-	**85**

Table 4: 3-Point Substrate Moisture Comparison

Specimen	Max Load (lbf)	Modulus of Rupture (psi)
Substrate	1997.4	985
98% RH	693.2	340
80% RH	903.2	430
10% RH	1066.5	500

The results from the 3-point flexure testing produce two key findings: 1) a substantial decrease in flexural strength exists when overlay material is applied to the substrate and 2) an increase in flexural strength is observed at lower substrate moisture conditions. From *Tables 3 and 4* it can be seen that the OTZ has significantly impacted the flexural strength of the substrate-repair concrete specimens. The plain substrate specimen demonstrated almost double the flexural strength of the substrate-repair concrete samples at all substrate moisture conditions. Additionally, there appears to be an increase in strength as the moisture condition of the substrate decreases. This observation would agree with published research that has demonstrated decreased shear strength in materials that were prewetted or moistened prior to casting [7, 10].

Table 5 presents the results of the 4-point flexural strength testing, and *Table 6* displays a comparison of the averages from each substrate moisture condition tested. Like the results from 3-point flexural testing, there remains a significant reduction in flexural strength for substrate-repair specimens when compared to plain substrate. The substrate-repair concrete specimens subjected to 3-point flexure testing experienced an average reduction in Modulus of Rupture, M_R, of 57%. The average reduction in M_R for the 4-point flexural testing of all specimens was 62%.

Table 5: 4-Point Flexural Testing Results

Specimen	Test	Max Load (lbf)	Span Length (in)	Specimen Depth (in)	Specimen Width (in)	Modulus of Rupture (psi)
Substrate	1	2259.4	9.25	3.00	3.10	750
	2	2538.5	9.25	3.00	3.15	840
	3	2643.3	9.25	3.00	3.10	860
	Average	**2480.4**	-	-	-	**815**
	Std. Dev.	-	-	-	-	**60**
98% RH	1	429.2	9.25	3.05	3.10	140
	2	1437.5	9.25	3.10	3.05	470
	3	865.8	9.25	3.00	3.10	280
	Average	**910.8**	-	-	-	**295**
	Std. Dev.	-	-	-	-	**165**
80% RH	1	1153.8	9.25	3.10	3.15	355
	2	784.3	9.25	3.00	3.10	255
	3	1443.8	9.25	3.05	3.15	455
	Average	**1127.3**	-	-	-	**355**
	Std. Dev.	-	-	-	-	**100**
10% RH	1	954.3	9.25	3.00	3.10	315
	2	749.4	9.25	3.05	3.05	250
	Average	**851.9**	-	-	-	**285**
	Std. Dev.	-	-	-	-	**50**

Table 6: 4-Point Substrate Moisture Comparison

Specimen	Max Load (lbf)	Modulus of Rupture (psi)
Substrate	2480.4	815
98% RH	910.8	295
80% RH	1127.3	355
10% RH	851.9	285

Interestingly, the increase in M_R as substrate moisture condition decreases is not present in the 4-point testing. There is an increase in strength as the moisture condition decreases from 98% RH to 80% RH, however there is no subsequent increase when decreasing moisture condition further from 80% RH to 10% RH. It is important to note however that only two specimens were utilized for both 3- and 4-point loading for the 10% RH substrate moisture condition. Such a sample size would not provide adequate

data points for a complete statistical analysis and the results of the 3- and 4-point flexure tests can not sufficiently attribute an increase in M_R with reductions in substrate moisture condition.

Furthermore, the data presented in *Tables 5 and 6* display a wide range of peak loads and M_R for all moisture conditions. For example, the 4-point flexure test results for the 98% RH moisture condition demonstrate a range of peak loads from 429.2 lbf to 1437.5 lbf and a range of M_R from 140 psi to 470 psi. These results represent a coefficient of variation (CV) of 45.3% and 45.6%, respectively. This variation represents a wide range of results and would indicate that a larger sample size may be needed to identify any correlations between flexural strength and substrate moisture condition.

The below images show the OTZ of substrate-repair specimens after subjecting them to the 3-point flexure tests. These images are taken from a 98% RH specimen directly after testing. A visual inspection of these images will provide important observations related to aggregate gradation and adhesion along the OTZ.

Visual inspection of the interface between the substrate and repair material after flexural strength testing indicated the relative adhesion of the interface. In *Figure 44* the adhesion of substrate on the repair interface can be seen in the left specimen. The outlined red region is substrate concrete that adhered to the repair material. From literature reviewed in this thesis, it has been experimentally demonstrated that higher substrate moisture conditions produce greater adhesion between substrate and repair material [10]. As a result, it should be expected that the SSD (98% RH) specimen would develop the greatest adhesion between materials. Although this research did not quantify the level of adhesion between the materials, a visual inspection will demonstrate the minimal adhesion developed—even at the SSD condition. This reduced level of adhesion may be the reason for the large reduction in flexural strength experienced during these tests.

The image presented in *Figure 45* demonstrates the poor gradation of aggregate particles along the interface. On the left side of the image (the repair material) there is a lack of large aggregates. This gradation—where a higher concentration of fine aggregate particles disproportionally packs against the

substrate—has been published in previous literature evaluating the OTZ of substrate-repair concrete [1]. The poor gradation along the interface is due to the presence of the substrate material which prohibits efficient particle packing. This inefficient particle packing along the OTZ is analogous to the "wall effect" associated with the ITZ and was previously discussed in this thesis.

Figure 44: 98% RH Interface Adhesion. Repair (Left), Substrate (Right)

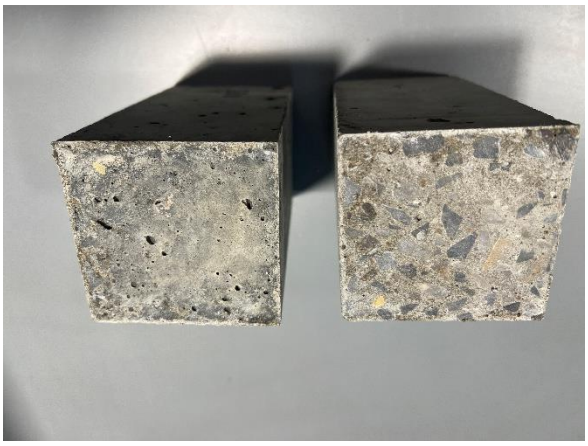

Figure 45: 98% RH Interface Aggregate. Repair (Left), Substrate (Right)

Fracture Energy Results and Discussion

During the RILEM fracture testing, the applied load is measured along with the critical mouth opening displacement (CMOD) of the induced notch. The load is continuously applied until loading has reached about 95% of the peak load and is then manually reduced. The specimen will unload until loading

is reduced to zero and the reloading begins. The slope of the initial loading period will be utilized to determine the initial loading compliance, C_i. After deriving the initial loading compliance, the Young's modulus (E) can be determined by utilizing the formula presented in *Equation 2*, where S is the span length, a_o is the initial notch depth, HO is knife edge thickness, C_i is the unloading compliance, d is beam depth, and b is beam thickness:

$$E_i = \frac{6Sa_0V_1(\alpha)}{C_i d^2 b} \tag{2}$$

$$V_1(\alpha) = 0.76 - 2.28\alpha + 3.87\alpha^2 - 2.04\alpha^3 + \frac{0.66}{(1-\alpha)^2} \tag{3}$$

$$\alpha = \frac{\alpha_o + HO}{d + HO} \tag{4}$$

After determining the modulus and initial compliance, the unloading compliance can be determined from evaluating the slope along the linear portion of the unloading curve. After determining the slope of this line, the unloading stiffness (E_u) can be calculated:

$$E_u = \frac{6Sa_cV_1(\alpha_c)}{C_u d^2 b} \tag{5}$$

By setting the initial and unloading stiffnesses equal, the critical effective crack length (ac) can be determined:

$$a_c = a_o \frac{C_u V_1(\alpha_o)}{C_i V_1(\alpha_c)} \tag{6}$$

After determining the critical effective crack length, initial and unloading compliances, the critical stress intensity factor (K_{Ic}) can be determined, where $\alpha = a_c/d$, P_{max} = measured maximum load, $W = W_oS/L$, and W_o = beam self-weight.

$$K_{Ic} = 3(P_{max} + 0.5W)\frac{S\sqrt{\pi a_c}F(\alpha)}{2d^2 b} \tag{7}$$

$$F(\alpha) = \frac{1.99 - \alpha(1-\alpha)(2.15 - 3.93\alpha + 2.7\alpha^2)}{\sqrt{\pi}(1+2\alpha)(1-\alpha)^{3/2}} \tag{8}$$

Next, the critical crack tip opening displacement ($CTOD_c$) can be determined:

$$CTOD_c = \frac{6P_{max}Sa_cV_1\alpha}{Ed^2b}[(1-\beta)^2 + (1.081 - 1.149\alpha)(\beta - \beta^2)]^{\frac{1}{2}} \quad (9)$$

The initial fracture energy (G_{Ic}) is the strain release rate and can be determined by:

$$G_{Ic} = \frac{{K_{1c}}^2}{E} \quad (10)$$

After determining the initial fracture energy, the total fracture energy (G_F) can be determined by removing the unloading portion of the load vs. CMOD curve and calculating the total area under the curve. A is the area under the curve, δ_f is the deflection at failure with zero load:

$$G_F = \frac{A + \frac{W_o S}{L}\delta_f}{(d - a_o)b} \quad (11)$$

After completing the RILEM fracture testing for all specimens, the load vs. CMOD data was graphed. The graphs for all substrate moisture conditions and specimens are presented in *Figures 46, 47, 48, and 49*:

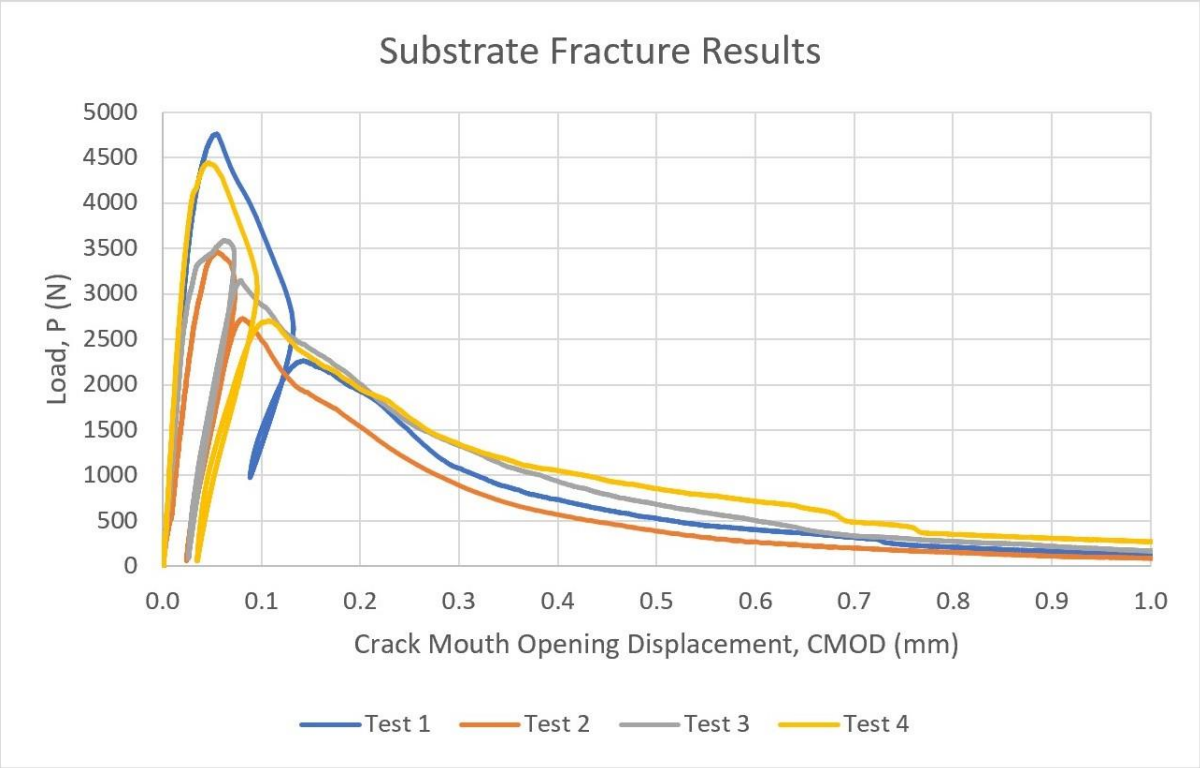

Figure 46: Substrate Fracture Results

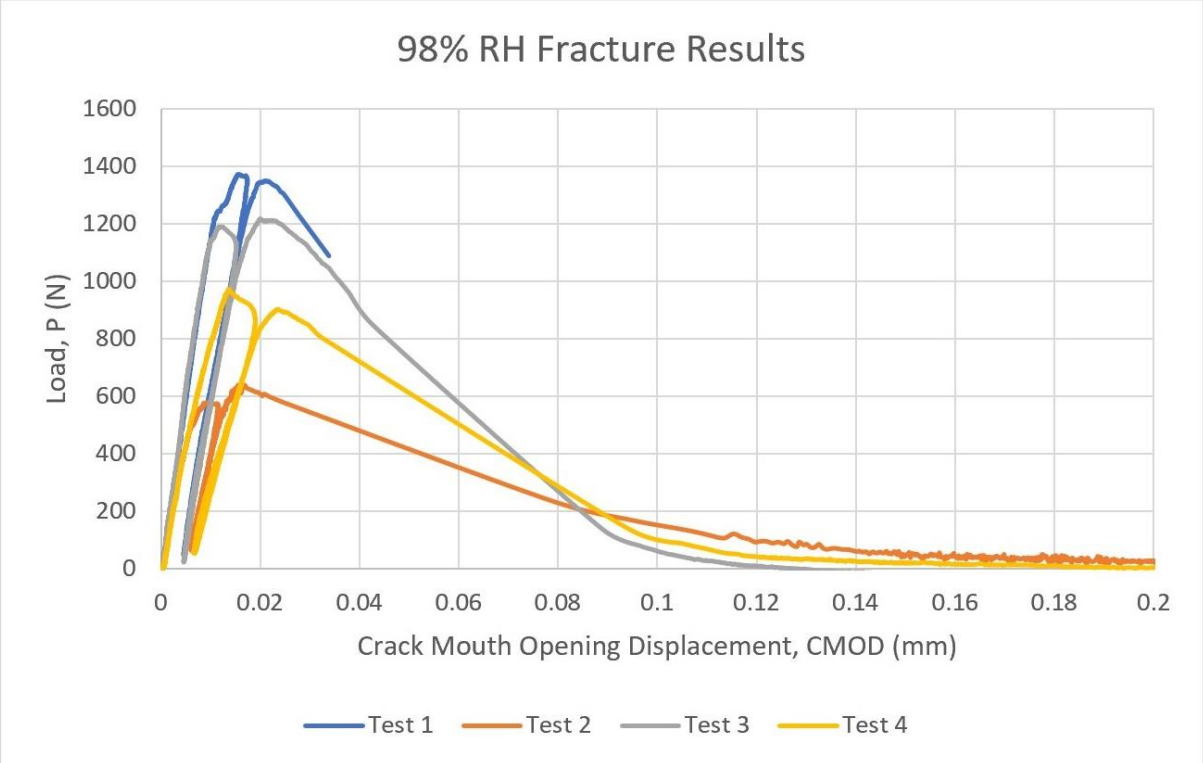

Figure 47: SSD (98% RH) Fracture Results

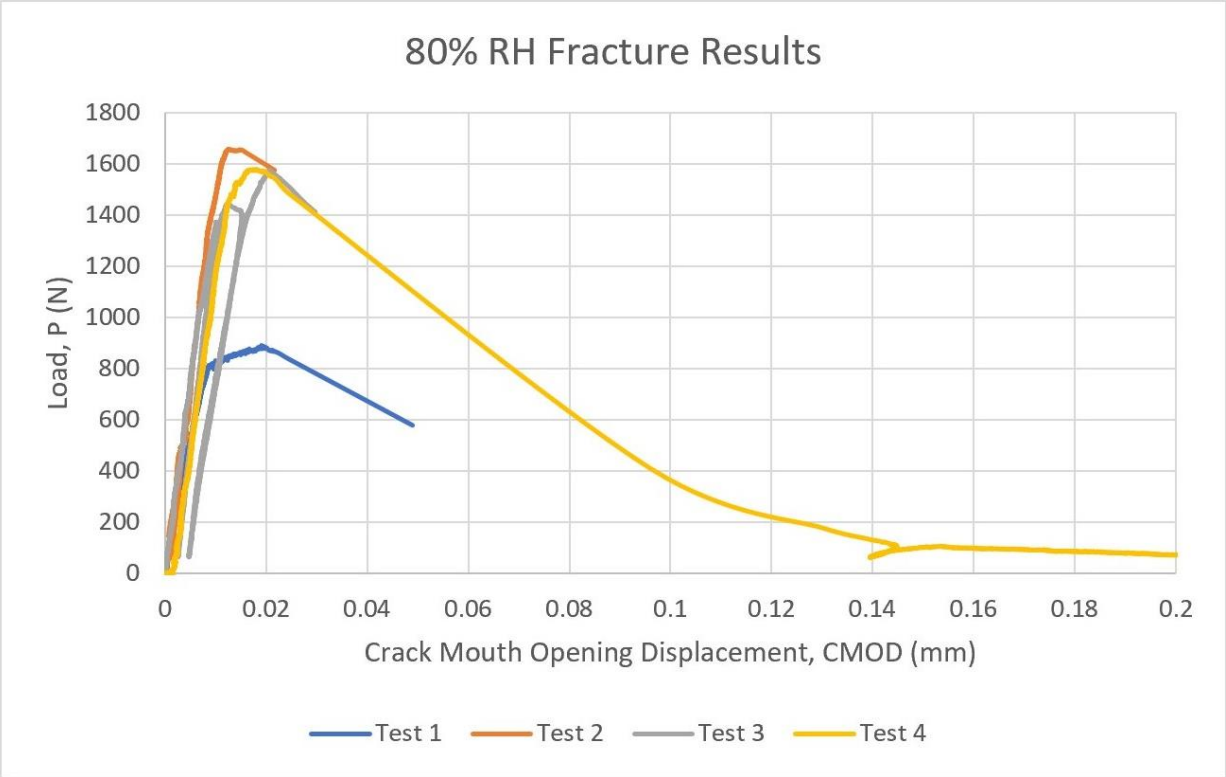

Figure 48: Sub-SSD (80% RH) Fracture Results

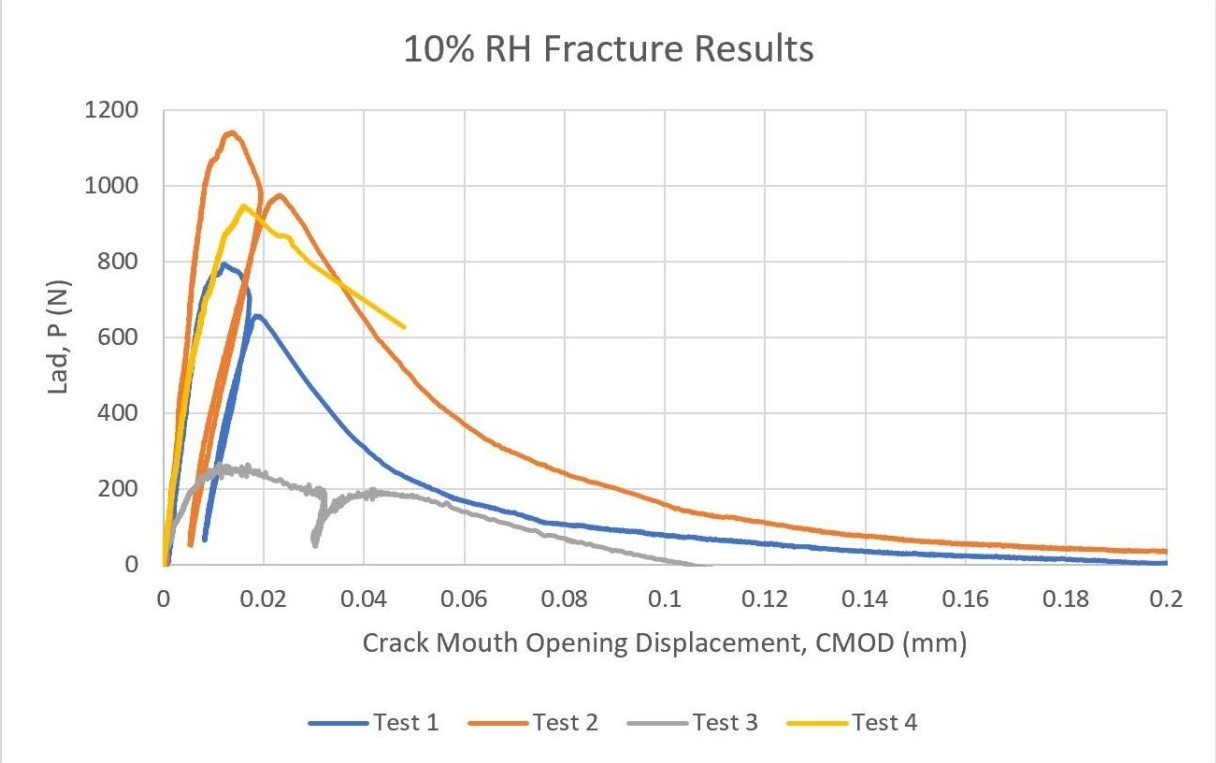

Figure 49: OD (10% RH) Fracture Results

After plotting the load vs. CMOD curves, the fracture parameters were determined. *Tables 7* and *8* display the results of the RILEM fracture testing. It is important to note that throughout the testing, a few specimens failed prior to completing the test method. These specimens are identified in the data presentation. A summary of the average values for each substrate moisture condition is provided in *Table 8*.

Table 7: RILEM Fracture Results

Substrate Condition	Beam No.	Peak Load, P_{max} (kN)	Modulus, E (GPa)	Critical Stress Intensity Factor, K_{Ic} (MPa-$m^{1/2}$)	Critical Crack Tip Opening Displacement, $CTOD_c$ (mm)	Initial Fracture Energy, G_{Ic} (N/m)	Total Fracture Energy, G_F (N/m)
Substrate	1	4.76	27.7	2.117	0.0680	161.7	244.1
	2	3.46	28.3	1.249	0.0235	55.1	138.9
	3	3.58	23.6	1.034	0.0247	45.2	161.3
	4	4.45	33.7	1.879	0.0465	104.8	242.0
	Avg.	4.06	28.3	1.570	0.0407	91.7	196.6
	COV	15.7%	14.6%	32.6%	51.8%	58.3%	27.7%
SSD (98% RH)	1	1.37	25.9	0.355	0.0049	4.9	14.1
	2	0.64	19.0	0.168	0.0023	1.5	13.8
	3	1.22	24.9	0.315	0.0049	4.0	10.2
	4	0.93	17.9	0.271	0.0060	4.1	11.1
	Avg.	1.04	21.9	0.277	0.0045	3.6	12.3
	COV	31.1%	4.1%	29.0%	34.7%	40.6%	15.8%
Sub-SSD (80% RH)	1[1]	0.89	15.9	-	-	-	1.26
	2[1]	1.66	28.3	-	-	-	1.33
	3[2]	1.58	23.1	0.331	0.0040	4.7	4.7
	4[1]	1.58	26.1	-	-	-	24.3
	Avg.	1.43	23.4	-	-	-	-
	COV	21.8%	20.1%	-	-	-	-
OD (10% RH)	1	0.79	21.5	0.234	0.0048	2.6	8.1
	2	1.14	29.8	0.420	0.0087	5.9	14.3
	3	0.27	8.0	0.088	0.0029	1.0	4.1
	4[1]	0.95	18.0	-	-	-	1.2
	Avg.	0.79	19.3	0.247	0.0055	3.2	6.9
	COV	47.6%	46.7%	67.3%	54.1%	78.9%	81.9%

1. Specimen failed while unloading. No unloading compliance can be determined.
2. Specimen experienced three progressively higher peaks, then failed during unloading.

Table 8: Average RILEM Fracture Results

Substrate Condition	Peak Load, P_{max} (kN)	Modulus, E (GPa)	Critical Stress Intensity Factor, K_{Ic} (MPa-$m^{1/2}$)	Critical Crack Tip Opening Displacement, $CTOD_c$ (mm)	Initial Fracture Energy, G_{Ic} (N/m)	Total Fracture Energy, G_F (N/M)
Substrate	4.06	28.3	1.570	0.0407	91.7	196.6
98% RH	1.04	21.9	0.280	0.0045	3.6	12.3
80% RH[1]	1.43	23.4	-	-	-	-
10% RH	0.79	19.3	0.247	0.0055	3.2	6.9

1. Since three specimens failed while unloading, average values cannot be determined.

Since a total of four (4) specimens failed during unloading, it is speculated that the bond strength between the substrate and repair material was inefficient and did not develop adequate strength to maintain adhesion through loading and unloading. After plotting the load vs. CMOD curves and tabulating the fracture parameters, the following observations were made:

1. There was a significant decrease in peak load, critical stress intensity factor, and fracture energies (initial and total) in the bonded substrate-repair materials.
2. The substrate-repair specimens experienced high coefficient of variations (COV), indicating a widespread in measured data. This highlights the unpredictability of fracture response for bonded overlays.
3. The COV increased for all fracture parameters when decreasing the substrate moisture condition from 98% RH to 10% RH. This may indicate an increase in unpredictability as substrate moisture conditions are reduced. An increase in unpredictability may reduce the desire to utilize the OD condition in field repairs since experienced results may vary widely.
4. The 80% RH moisture condition demonstrated very low bond strength, and this was attributed to multiple specimens failing prior to developing an unloading response in the material.
5. Fracture testing produced no statistically significant response between any substrate moisture condition.

To further explore the implications of the fracture testing results, *Figures 50, 51, and 52* display the failure planes for different specimens.

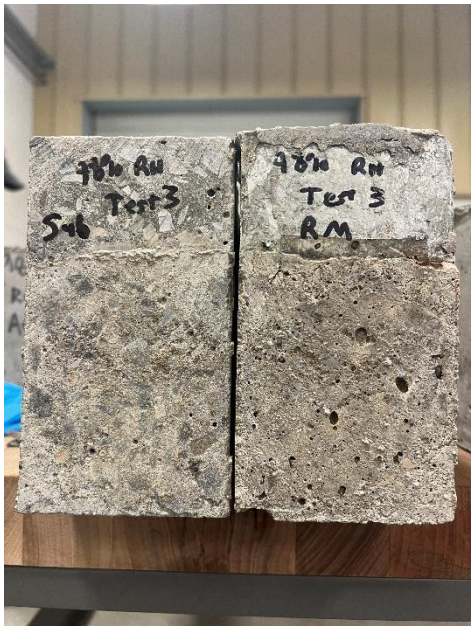

Figure 50: 98% RH Fracture Plane. Repair (R), Substrate (L)

Figure 51: 80% RH Fracture Plane. Repair (L), Substrate (R)

Figure 52: 10% RH Fracture Plane. Repair (R), Substrate (L)

After completing a visual inspection of *Figures 50, 51, and 52*, additional observations can be made:

1. All specimens failed directly through the OTZ of the substrate-repair bond. This indicates that there was not enough adhesion between the materials to facilitate failure in the bulk concrete.
2. Very little adhered concrete remains on the substrate surface for all moisture conditions.
3. Adhered concrete can be seen on the bottom of the repair material in the 80% RH sample (*Figure 51*). This specimen was Test 3 and was the only specimen for this moisture condition that was able to complete the RILEM fracture testing. The increased adhesion may explain why this sample was able to demonstrate more favorable results.
4. There is improper gradation at the interface of the repair material for all substrate moisture conditions. When inspecting the substrate half of the specimens, large aggregates are visible on the surface. However, for the repair material little to no large aggregates appear. This would highlight the improper gradation (due to inefficient particle packing as a result of the "wall effect") that is discussed in published literature [1].

Since the test method experienced bonding failures and a statistically insignificant sample size was utilized, further fracture testing may be beneficial in establishing optimum substrate moisture condition for this test method.

Rapid Chloride Penetration Testing (RCPT)

After batching RCPT pucks in accordance with the mix design proposed in *Table 1*, it was observed that several specimens for the 80% RH moisture condition cured with an oblong geometry. It is assumed that since both materials were batched in separate events utilizing plastic molds, that one side of the material was allowed to expand more than the original material. This created the oblong shape displayed in *Figure 53*.

Figure 53: 80% RH Failed Puck

Since RCPT requires the substrate-repair puck to be placed inside of a rigid cell, the oblong shape would not allow the insertion of the puck. A significant effort was made to grind down the puck so that the specimen can fit inside of the cell. After grinding the puck and applying the two-part epoxy, it was determined that although the puck would fit inside of the cell, the geometry would not allow a proper seal and would cause the NaOH and NaCl solutions to leak from the cell during testing. Therefore, it was determined these pucks would not be sufficient for testing and that repeating the batch event was necessary. Although the 80% RH pucks were not usable, the pucks for the other moisture conditions were

found to be suitable and the standard testing was performed on them. The results of this test are provided in *Table 9*.

Table 9: Initial RCPT Results

Moisture Condition	Average Charge Passed (C)	Standard Deviation (C)	Penetrability Risk
Substrate	5501	674	High
98% RH	3989	734	High
10% RH	5212	710	High

The chloride penetrability risk mentioned above is defined by ASTM C1202 and is designated by the total charge passed through the specimen during testing. An overview of the penetrability risk associated with the ranges of passed charge is presented in *Table 10*.

Table 10: Chloride Ion Penetrability Risk Based on Charge Passed (C)

Charge Passed (C)	Chloride Ion Penetrability
> 4,000	High
2,000 – 4,000	Moderate
1,000 – 2,000	Low
100 – 1,000	Very Low
< 100	Negligible

After completing the RCPT test for the acceptable pucks, efforts moved to batch new substrate-repair material cylinders. During this batching period the RCPT cell was placed around the cylinders to ensure the geometry was maintained during the curing period. The specimens were made and cured according to the guidelines outlined in Section 3.2 Methods and Procedures. Unfortunately, after batching the 98% RH and 80% RH cylinders, the environmental chamber began experiencing mechanical failures. Due to the status of the environmental chamber, the 10% RH substrate-repair material specimens were unable to be cast. Since the 10% RH RCPT testing was already performed in the initial testing sequence, it was decided to proceed testing with the other samples. The results of the second RCPT testing are displayed in *Table 11*.

Table 11: RCPT Retest Results

Moisture Condition	Average Charge Passed (C)	Standard Deviation (C)	Penetrability Risk
Substrate	4029	797	High
98% RH	4505	717	High
80% RH	5015	760	High

After performing the second RCPT testing, the results from both initial and the retest were combined and averaged to develop an overall evaluation of chloride ion penetrability risk. The average results of the RCPT testing are presented in *Table 12*.

Table 12: RCPT Average Results

Moisture Condition	Average Charge Passed (C)	Standard Deviation (C)	Penetrability Risk
Substrate	4448	893	High
98% RH	4672	719	High
80% RH	5015	760	High
10% RH	5211	710	High

The averaged results tabulated above indicate an increase chloride ion penetrability risk as the substrate moisture condition decreases. These results agree with published literature:

- There is an increase in penetrability risk due to the OTZ between substrate-repair concrete. Published literature concluded that conductivity in the ITZ is approximately 10x greater than that of the bulk paste [46]. The ITZ is also known to have increased porosity due to the "wall effect" and decreased cement paste content [2].
- Dry substrates demonstrate greater porosity and higher voids than pre-wetted substrates [10, 41]. This relationship would explain the increase in penetrability risk as the substrate-repair pucks decrease in moisture condition from 98% RH to 10% RH.

The results of the RCPT testing for substrate-repair concrete indicate that the optimum level of substrate moisture condition is saturated surface dry (SSD). This condition would demonstrate improved

porosity and void content when compared to drier substrates, ultimately reducing the risk of chloride ion penetration.

3.4 Conclusions

To evaluate the optimum substrate moisture condition between substrate-repair concrete a series of flexural testing, fracture energy, and chloride ion penetration tests were performed. These tests included 3-point loading, 4-point loading, RILEM fracture energy, and rapid chloride penetration testing (RCPT). Since the objective of this thesis is to provide a correlation between measured properties and moisture condition, a review of the observed results is pertinent.

The results of the RILEM fracture energy test were too inconsistent to develop a statistically significant correlation between substrate moisture condition and fracture parameters. This test method also experienced premature failures in two out of three substrate moisture conditions, where complete fracture parameters could not be determined. The only conclusive observation that can be made after conducting the RILEM testing was that there is a substantial loss in fracture properties between substrate and substrate-repair specimens. The 98% RH and 10% RH specimens averaged a 65% and 81% reduction in measured maximum peak loads, respectively. This outcome suggests that the OTZ between substrate-repair concrete is the weakest zone of the specimen and would be in agreement with current published literature [9]. The decrease in measured peak load from 98% RH to 10% RH would seem to suggest that as moisture conditions decrease, the peak load decreases. However, the results of the 80% RH specimens displayed an overall increase in measured peak load when compared to the 98% RH samples. Since all the 80% RH samples failed at some point during the unloading portion of the test method, this correlation cannot be accurately made. Therefore, the results of the RILEM fracture testing do not provide any relationship between substrate moisture condition and fracture parameters.

The last substrate-repair test procedure was the RCPT. After analyzing the results of this test method, it can be observed that decreasing the substrate moisture condition will decrease the resistance of

the OTZ to chloride ion penetration. This observation agrees with current literature identifying an increase in porosity and voids associated with drier substrates [10, 41].

Upon completing the testing procedures outlined in this thesis, a positive correlation between substrate moisture condition and measured properties cannot be established for the following reasons:

1. Unreliable results: the results produced by the experiments were either inconsistent or did not demonstrate any statistical significance.
2. Sample size: due to adhesion failures, issues with the environmental chamber, and premature testing failures, a statistically insignificant number of samples were utilized in these experiments. At a minimum, three samples for each condition in each test method should be analyzed.

There are a few reasons to potentially describe the adhesion issues and inconsistencies in results. The first reason may have been a lack of apparent moisture on the substrate surfaces. Upon removing all samples from the environmental chamber, the surfaces appeared dry. Although each specimen was conditioned for approximately 18 ± 2 hours at the desired relative humidity, the surfaces did not maintain visible water. The general industry practice with pre-wetting substrates prior to the application of an overlay consists of either ponding the surfaces or spraying the substrates with water [3]. This technique would provide at least some water on the surface prior to overlay application. Additionally, when the substrate specimens were batched, cured, and then sawcut to prepare for repair material overlay, the samples would expand slightly towards the top of the sample. This made insertion of the substrate halves back into the molds difficult. The difficulty in inserting the substrate halves led to long waiting times before the repair material could be added to the mold. In the beginning of the research, it would take approximately 45 minutes to successfully insert substrate halves and batch repair material. During this time, it is suspected that the slight surface moisture maintained by the samples may have evaporated. In one study reviewed for this thesis, the authors suspected that their 20-minute batching period where substrates were exposed to ambient laboratory conditions was sufficient time for the substrate surface moisture to diminish [41]. Another possible cause of the challenges experienced in this study may be the surface roughening of the

substrates. All the substrate-repair samples were prepared by cutting the substrate specimens in half. After cutting the specimens, the remaining debris was cleaned off with no other surface preparations being performed. The literature reviewed for this thesis covered several surface roughening techniques consisting of sandblasting, hydro jetting, and grinding [10, 11]. Surface roughening is conducted to increase mechanical interlock between substrate and repair material and has been demonstrated to greatly improve pull-off and slant shear strengths [10]. Although performing surface roughening may extend the focus of the study beyond the direct involvement of substrate moisture condition, increasing mechanical interlock between the two materials may have been beneficial.

3.5 Future Work

To expand upon the research conducted in this thesis, further trials can be undertaken to evaluate substrate moisture condition with different conditioning methods. In this thesis the environmental chamber was utilized to condition the samples at a consistent relative humidity. As noted in previous sections, when these specimens were removed the surfaces presented with no visible moisture. Therefore, efforts can be made to explicitly saturate the surfaces to obtain desired moisture conditions. This effort would ensure apparent moisture remained on the surfaces for the saturated surface dry and sub-saturated surface dry specimens. Furthermore, efforts can be made to increase the mechanical interlock between the substrate-repair materials through some method of surface roughening. If the method of roughening were consistent across all specimens, the effect of substrate moisture condition would remain apparent throughout the experiments. Lastly, in future substrate-repair testing an increased sample size would be beneficial at identifying the statistical significance, if any, substrate moisture condition maintains.

Another area of importance of substrate-repair interfaces is understanding the ability of the OTZ to resist chloride ion diffusion. In future research, substrate-repair specimens can be made with varying substrate moisture conditions and evaluated utilizing transmission X-ray microscopy. This technique would supplement any rapid chloride penetrability testing and provide a more in-depth understanding of diffusivity along the substrate-repair interface. Since this test method is non-destructive, scans can be

obtained throughout the curing period and would provide an alternative perspective when determining ion penetration risk. This analysis may be able to identify optimum substrate moisture condition and desired curing period for optimum penetration resistance.

4. Section 2: X-Ray Computed Tomography (XCT) and Dental X-Ray (CHIP)

4.1 Background

The Thomas M. Murray Structures and Materials Laboratory at Virginia Tech maintains a SkyScan 1174 μCT scanner. This scanner can obtain radiographs with an estimated resolution between 6 and 30 μm. Unfortunately, this scanner was unused for several years after acquisition in 2005 and its overall condition was unknown. Therefore, the bulk of the XCT research for this thesis was dedicated to bringing the scanner back into operation. This included creating and scanning test specimens, reconfiguring scanner settings, incorporating filters, and consulting with the product manufacturer. An image of the SkyScan 1174 scanner is presented in *Figure 54*.

Figure 54: SkyScan 1174 μCT

For the test specimens, there were three trial runs conducted on two separate materials. Two of the three specimens scanned were of the same mix design but were scanned at different periods under various scanner settings. The third specimen was a concrete core obtained from the samples in the substrate-repair concrete research portion of this thesis. The mix design for this concrete is documented in Section 3.1, Table 1: Concrete Mix Design for 1 yd^3. The other two specimens were mortar samples created to develop calibration curves to conduct transmission X-ray microscopy (TXM). As such, samples were created with varying concentrations of potassium iodide (KI). These samples were made in

accordance with ASTM C305 [47]. As discussed in the literature review portion of this thesis, potassium iodide (KI) is utilized as a tracer due to its high atomic mass. The samples will absorb a varying number of X-rays depending on their KI concentration. The number of absorbed X-rays will alter the level of gray values depicted in the radiograph. From there, image analysis can be performed to associate KI concentrations with specific gray values, ranging from 0 to 255. The mix design and specific KI concentrations are displayed in *Table 13.*

Table 13: Cement Mortar Mix Design

KI Concentration (%)	Cement (g)	Water (g)	Sand (g)	KI (g)
0	891.00	400.95	1399.61	0.00
1	356.40	160.38	559.84	1.60
2	356.40	160.38	559.84	3.21
4	356.40	160.38	559.84	6.42
6	356.40	160.38	559.84	9.62
8	356.40	160.38	559.84	12.82
10	356.40	160.38	559.84	16.04

Section 4.2 Methods and Procedures will discuss the completed steps to prepare the specimens for scanning, the configuration of scanner settings, and other efforts in restoring the μCT.

After attempts to restore the SkyScan 1174 scanner were complete, efforts transitioned to researching and designing the dental X-ray "CHIP" system. The initial efforts for constructing the CHIP system were to review the NCHRP Idea Project report and coordinate with one of its authors, Dr. Amir Behravan [25]. The system requires two major components, a dental X-ray source and a sensor. In the original CHIP system, a Gendex GX-770 was utilized as the X-ray source. The sensor for the system was a Schick 33. After researching the various X-ray sources and sensors commercially available, the CHIP system in this study used a Gendex Expert DC X-ray source and a Vatech HD Sensor (Size 2). Since the objective of the system is to obtain optimum resolution in the radiographs, the Expert DC model was chosen due to its 0.4 mm focal point. Comparatively, the GX-770 maintains a focal point of 0.6 mm. By reducing the focal point, a better resolution should be expected. Furthermore, the HD sensor was selected due to its high resolution as well. The other components associated with CHIP construction were

commercially available and are discussed in Section 4.3, where a description of the equipment as well as a schematic of the build is provided.

4.2 Methods and Procedures

Though the XCT and CHIP research projects consist of tracking chloride ion diffusion through transmission X-ray microscopy (TXM), the required methods and procedures outlined for each project are significantly different. For the XCT project, the goal of the research was to optimize the SkyScan 1174 scanner so that TXM can be performed at Virginia Tech. On the other hand, the CHIP project was initiated to develop an X-ray scanner utilizing dental X-ray equipment. The methods and procedures for the CHIP system were to review the NCHRP paper and coordinate construction with Dr. Behravan. Since the methods and procedures for the XCT are more involved, they are outlined below. For the CHIP system, the design and schematics are displayed in Section 4.3 Results and Discussion.

X-ray Computed Tomography (XCT)

The first requirement prior to beginning XCT experiments was to create the mortar samples according to the mix design presented in *Table 13*. Samples were created with KI concentrations ranging from 0-10%. The radiographs of these samples would be utilized to generate a calibration curve, which is used to derive an apparent diffusion coefficient. An image of the samples for calibration are displayed *Figure 55.*

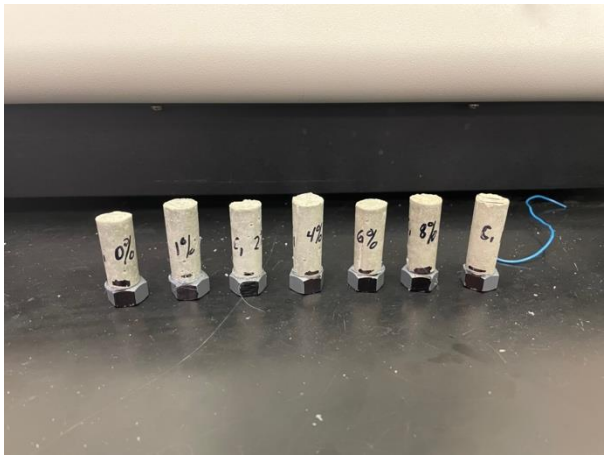

Figure 55: XCT Calibration Samples

Once the mortar samples were created, they were placed into the fog room to begin curing. There were two initial challenges associated with the SkyScan 1174. First, the scanner has not been operated in several years and it was unknown whether the X-ray source would be strong enough to penetrate the samples. If the X-rays were unable to penetrate the samples, ion tracking would not be possible. Secondly, TXM had not been a technique employed by the laboratory with this scanner. Therefore, the required settings were unknown and needed to be configured. To ensure safety, the manufacturer of the scanner was contacted to perform a safety inspection. This was to ensure there were no X-ray leaks from the scanner. Once the scanner was verified to be leak-free, efforts to conduct TXM resumed. The first component needed for TXM was a stage. The stage would be the placeholder for specimens and would ensure proper orientation between each scan. Since TXM is attempting to track ion diffusion, the diffusion front would need to be oriented in the same manner during every scan as the specimen ages. This is because diffusion will not occur uniformly through the samples and its progress will be affected by pores located throughout the microstructure. Since TXM had not been performed using this scanner, a custom stage needed to be designed. After taking measurements inside of the scanner, a 3D stage was designed utilizing computer-aided design (CAD). Once the stage was designed, it was printed by the Prototyping Studio in the Virginia Tech Library. *Figure* 56 is the 3D stage designed for this project. Refer to Appendix A for dimensions and alternative views.

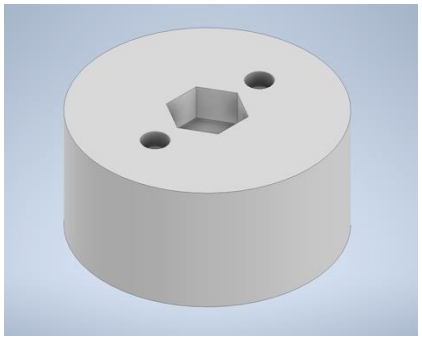

Figure 56: 3D Stage Design

The stage was marked to annotate “left, right, and front” so the specimen may be loaded the same way prior to each scan. An insert in the center of the stage was designed to accommodate a 3/8” PVC nut. The nut allowed the sample to sit firmly into the stage and ensured consistent sample orientation between scans. After creating the stage, the settings on the SkyScan scanner were modified to identify the best options for TXM. The settings altered for the initial scans are as follows:

- Camera size: small
- Pixel size: 33.5µm
- Exposure time: 1,950ms
- Geometrical Correction Option: checked
- Flat Field Correction Option: checked

Another option explored when attempting to obtain radiographs was the incorporation of a filter. The SkyScan scanner allows for the placement of a thin sheet of copper between the X-ray source and sample. However, the scanner did not maintain a method of securing the filter inside of the scanner. CAD was utilized to design a 3D filter holder, and it was printed using the Prototyping Studio. An image of the design is presented in *Figure 57*. Refer to Appendix A for dimensions and alternative views.

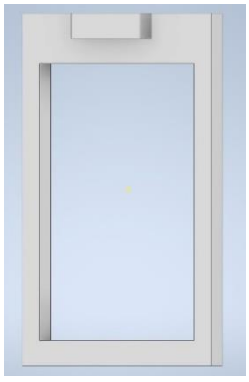

Figure 57: 3D Filter Holder Design

Once the stage, filter holder, and initial settings were configured, the research became an iterative process of scanning, changing settings, and rescanning to determine if the obtained radiographs were acceptable. As such, the methods and procedures between each scan will be discussed in the next section, Section 4.3, where the steps, results, and modifications are reviewed.

4.3 Results and Discussion

X-ray Computed Tomography (XCT)

After all required components were created and settings modified, the specimens needed to be prepared for scanning. To accurately track diffusion, there was a need to control direction so that diffusion only occurred through the top of the specimen. This required the application of a hydrophobic wax on all sides of the samples, excluding the top. The wax utilized was W-445 manufactured by Sonneborn. Once applied, the sample can be glued to a PVC nut. The PVC nut will fit into the top of the stage and will act as a place holder. A figure of the sample with wax and nut is presented in *Figure 58*. The nut was also marked in the front so that the sample can be loaded into the stage in the same position for each scan.

Figure 58: XCT Samples with Wax and PVC Nut

After preparing the samples, they were submerged in vials with a 0.6 mol/L KI solution for 6-days. After the ponding period the samples were removed and placed into the μCT scanner to obtain radiographs. The images below display the radiographs for the 0% and 10% KI concentrations. Since KI is utilized as a tracer, the 10% concentration samples would be expected to be darker, representing the increased concentration of KI.

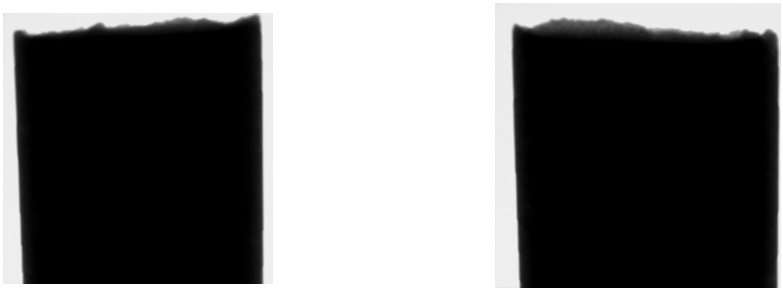

Figure 59: 0% (Left) and 10% (Right) KI Radiographs

From the images in *Figure 59* there appear to be no gradient in gray value and both images have a solid black image. These images can be compared with radiographs from published literature to identify expected results. From *Figure 60*—taken prior to the removal of background attenuation—the diffusion can be seen as the darker gray color proceeding down the sample as the ponding period increased.

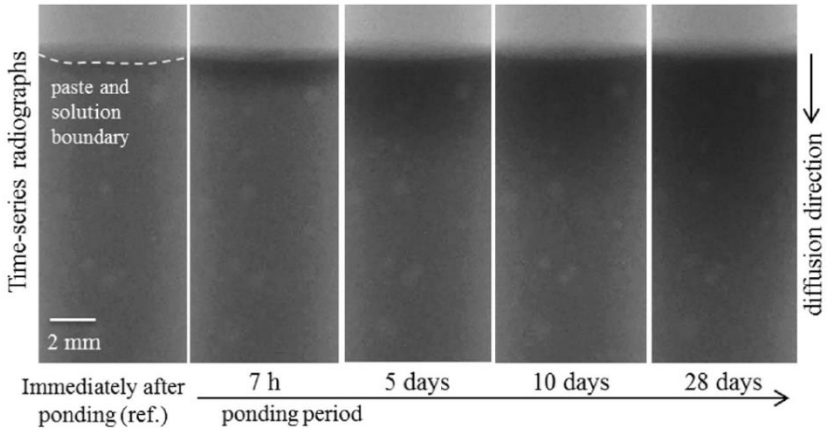

Figure 60: Time-Series Radiograph [16]

It is noted that *Figure 60* is not from a sample created for calibration with consistent KI concentration but is from a sample after ponding with KI solution. However, the difference in gray values represents the gradation that should be present between samples containing 0% and 10% KI. After receiving the results in the above figure, it was decided to reconfigure the settings on the scanner and reattempt the process. The scanner exposure setting was modified from the original 1,950 ms to 25,000 ms. The exposure time is increased to allow the sample to be exposed to a greater number of X-rays. This was intended to increase absorbed X-rays and ideally generate a more distinct contrast in grayscale values. The samples utilized for this series of scanning were from the batch prepared for the initial scans. At this point the specimens were cured for 9 weeks. *Figure 61* displays the obtained radiographs for 0% and 10% KI concentrations, respectively.

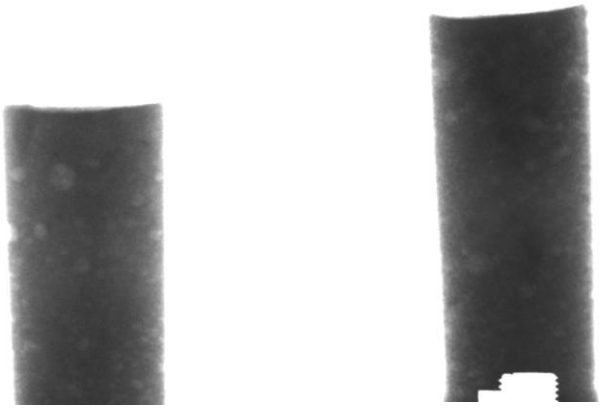

Figure 61: 0% (Left) and 10% (Right) KI Radiographs – 2nd Attempt

After imaging processing, it was noted that the gradient gray values were still not sufficient for producing an accurate calibration curve. From there, the copper filter was placed into the scanner and radiographs were obtained for all concentrations. The addition of the filter is to filter out lower energy X-rays and increase mean beam energy. The images below display the radiographs for both 0% and 10% KI concentrations with the filter in-place.

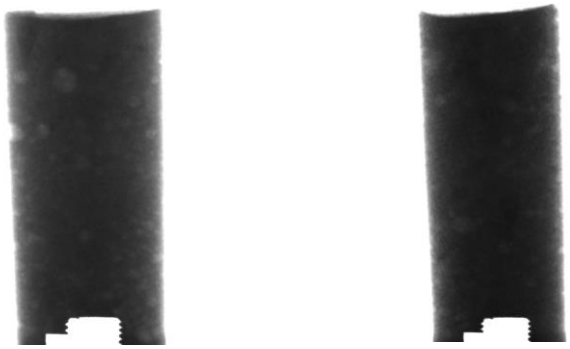

Figure 62: 0% (Left) and 10% (Right) KI Radiographs with Filter– 3rd Attempt

The results displayed in *Figure 62* display similar results to the radiographs with no filter—gray values are not sufficient for development of an accurate calibration curve.

From there it was decided to manipulate the Flat Field References and Geometrical Correction settings. The four options explored with these settings are as follows:

- Option 1: Flat Field References and Geometrical Correction options selected.
- Option 2: Only select the Geometrical Correction option.
- Option 3: Unselect both Flat Field References and Geometrical Correction options.
- Option 4: Only select the Flat Field Reference option.

To evaluate these options, two separate trial runs were conducted to obtain radiographs. These two trial runs are outlined below:

- Trial 1: ponded four samples with KI solution. Samples were from the initial cast date and were labeled M1-1, M1-2, T1-1, and T1-2.
- Trial 2: ponded 2 concrete cores with KI solution. The cores obtained from the substrate-repair concrete project with a w/c ratio of 0.45.

After ponding the samples, radiographs were obtained for each, and the data was analyzed. The obtained radiograph for all samples is provided in *Figures 63, 64, and 65*.

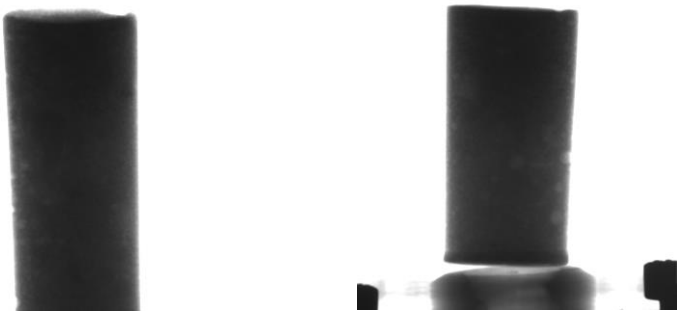

Figure 63: 14-Day Radiograph. M1-1 (Left), M1-2 (Right)

Figure 64: 14-Day Radiograph, T1-1 (Left), T1-2 (Right)

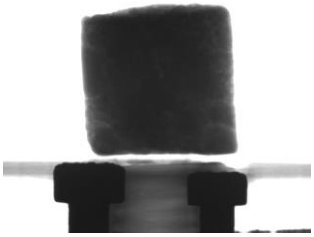

Figure 65: 5-Day Radiograph, Concrete Core

As can be seen from *Figures 63, 64, and 65* the radiographs still appear too dark to obtain accurate grayscale values. However, to verify this assumption the grayscale values were graphed, to determine if diffusion can still be tracked even if visual tracking remained difficult. After the initial image analysis Options 1 and 2 were eliminated because there was a change in gray value towards the bottom of samples. Since these samples were ponded with the KI solution, the only change in gray value should be

associated with diffusion, or penetration of the solution. If there is an observed change in gray value well-beyond what would be reasonably assumed as penetration, it would indicate inconsistent results and prevent the accurate derivation of a diffusion coefficient. Next, Options 3 and 4 were further analyzed to determine if the X-ray source can efficiently penetrate the sample and track diffusion. The graphs comparing Options 3 and 4 for sample T1-1 are presented in *Figures 66 and 67*.

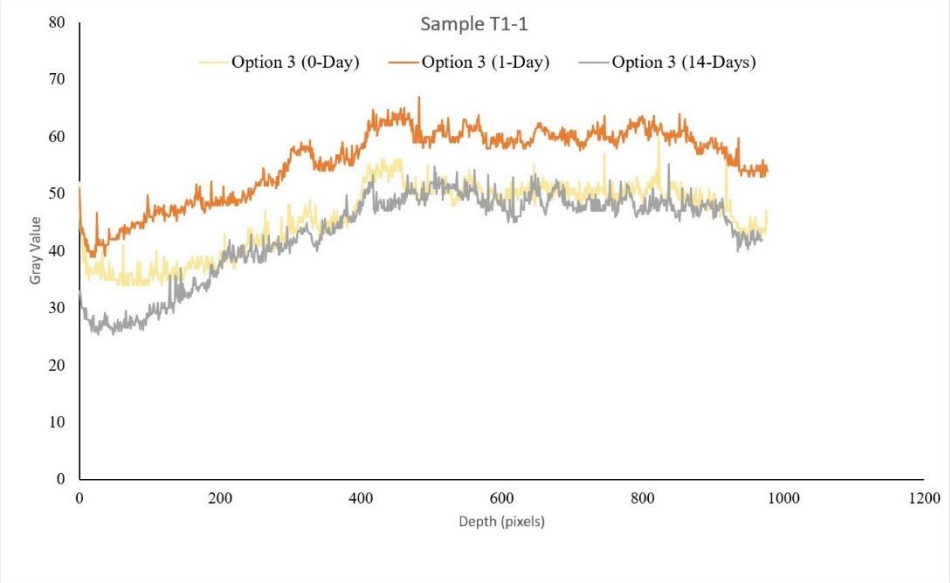

Figure 66: Sample T1-1 Time-Series Radiograph, Option 3

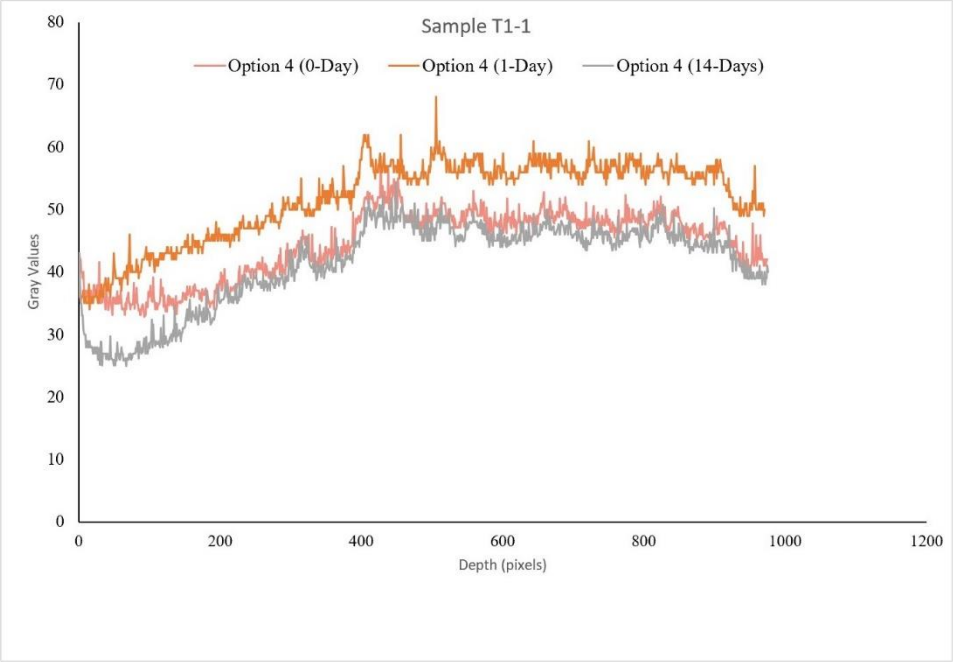

Figure 67: Sample T1-1 Time-Series Radiograph, Option 4

The image analysis software utilized in this portion of the project assigns a numeric value to represent the 8-bit level of grayscale in each pixel in the image. The values range from 0 to 255, with black being represented by 0 and white being represented by 255. Therefore, the darker the image, the lower the grayscale values. Since the KI solution should be absorbing the X-rays, the regions of the samples that have KI solution should appear darker, or have a lower grayscale value, than regions where diffusion has not yet occurred. The graphs in the image above begin at a distance of 0 pixels from the top of the sample and progress down the sample one pixel at a time. If the obtained radiographs were able to accurately track diffusion, then there should be darker values associated with lower pixel values and they should be increasing in grayscale value as the depth of the pixels increase. The increase in grayscale value would represent the decreased concentration of KI solution as the depth of the sample increase. In the graphs above it does appear that the X-ray was able to identify KI solutions near the surface of the sample. However, the graphs also depict an increase in grayscale value between the 0-day and 1-day scans. These results would indicate that concentrations decreased on the surface of the specimen from 0-

to 1-day. Since the concentration of the solution did not change, this indicates an unstable X-ray source and would suggest the scanner may not efficiently track diffusion.

One of the primary goals of the XCT research project was to couple the efforts of this research with the substrate-repair project. This would include obtaining concrete cores from the substrate-repair interface so that TXM could be performed to determine if the substrate moisture condition had a significant impact on diffusion in the samples. Since this remained a goal of the project, one final sample batch to scan in the SkyScan μCT. This batch was made with cement mortar and was intended to be used in developing a calibration curve. The mix design was made like the mix design in the substrate-repair project except for using no coarse aggregates. The mix design for the final test batch is presented *Table 14*.

Table 14: Cement Mortar Mix Design - Final Trial

KI Concentration (%)	Cement (g)	Water (g)	Sand (g)	KI (g)
0	125.06	63.30	197.30	0.00
1	125.06	63.30	197.30	0.56
2	125.06	63.30	197.30	1.13
4	125.06	63.30	197.30	2.25
6	125.06	63.30	197.30	3.38
8	125.06	63.30	197.30	4.50
10	125.06	63.30	197.30	5.63

After allowing these samples to cure, they were prepared for scanning by adding the PVC nut to the bottom. Unfortunately, during the scanning process of these samples the SkyScan 1174 was unable to consistently obtain radiographs. The software for the scanner would time out and quit prior to obtaining radiographs. Since the scanner was not able to retrieve the radiograph and with the given inconsistent results of previous experiments, the manufacturer of the system was contacted. Through conversations with the manufacturer, the following conclusions were made:

- An exposure setting of 25,000ms was extremely high and likely the source of software issues.
- The X-ray source in the scanner was not designed to penetrate samples with densities as high as mortar and concrete.

- Repair options were cost prohibitive. The options discussed were:
    - Replacing the tube to increase resolution: $60-70k for new parts.
    - Replacing tube with older, cannibalized parts: $10k+ for scanner recalibration. It was also noted that replacement of the tube may not eliminate the issues.
    - Purchase new µCT scanner: $300-400k.

Given the inconsistency in results and the extensive costs associated with repair or replacement, it was decided to discontinue efforts at restoring the SkyScan 1174 µCT scanner.

Dental X-ray (CHIP) System

After receiving the X-ray source and sensor described in Section 4.1, additional parts were needed for construction. These parts included hinges, safety switch, door locks, and lead lining. The lead lining will safeguard system operators and ensure X-rays are not released from the box. Next, the X-ray source received from the distributor was still attached to the arms normally utilized in a dental office environment. Since the arms were still attached, the wiring for the source was located throughout the arms and attached to the panel. This required the removal of the wiring from the arms to construct a box around the source. However, to perform this, the wiring for the source needed to be cut and soldered back together once removed from the arms. After removing the wiring, construction of the box began. A schematic of the box, with associated components is presented in *Figure 68*.

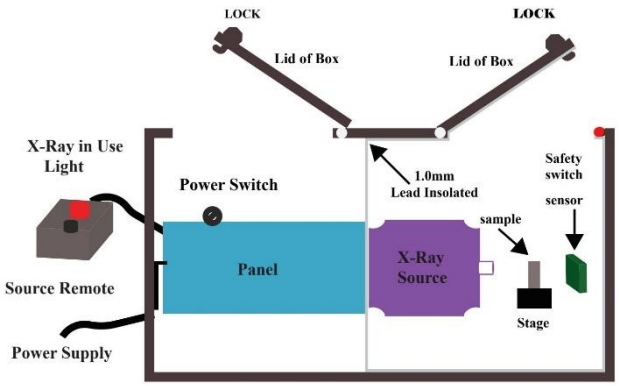

Figure 68: CHIP System Schematic

The system will house the operation panel in the left portion of the box, with the X-ray source and sensor on the right. The source, sensor, and stage will be fixed, to ensure constant distance between all components. Both sides of the box will have doors, secured by locks on the top. On the right side there is a safety switch that closes the circuit to the power source when the door is open, preventing operation while the X-ray is powered on. When the door closes, the circuit is opened, and the X-ray will be functional.

After developing the above schematic, construction on the CHIP system began. *Figures 69 and 70* display recent construction updates to the system. The initial construction on the box housing the equipment was completed. In *Figure 70*, the panel and X-ray source can be viewed. The X-ray source was placed on top of foam that will ensure the source remains stationary and provide some protection. The next construction steps will include adding the XCT stage, sensor, and covering the inside of the box with lead lining.

Figure 69: CHIP System (Outside)

Figure 70: CHIP System. Panel (L), X-ray Source (R)

4.4 Conclusions

Transmission X-ray microscopy is an effective and precise technique that provides characterization of transport properties in materials. It allows specimens to be nondestructively scanned and analyzed to determine chloride ion penetration risk. This observation can provide significant insight into the life expectancy of a structure and the effectiveness of various binders and surface sealers. As discussed in this thesis, TXM has been utilized to evaluate several different types of cement and cementitious materials. The results of these studies demonstrate TXM can efficiently track ion diffusion

and that potassium iodide is an effective tracer agent in modeling chloride diffusion [23]. Furthermore, the NCHRP Idea Project report reveals the ability of the CHIP system to conduct TXM experiments [25]. Given the affordability of the CHIP system, universities will be able to incorporate TXM experiments without the need of costly μCT scanners.

4.5 Future Work

Since incorporating used dental equipment is a recent approach to TXM, most future research will revolve around enhancing the system. These efforts may include designing a system that is more rugged and deployable for field use. Another improvement may be to enhance the scanning capabilities of the X-ray source and sensor to include specimens with larger diameters. Larger diameter samples may be more representative of samples currently obtained on project sites.

5. Section 3: Freeze/Thaw Conditions on Substrate-Repair Concrete

5.1 Background

To expand on the research conducted in Chapter 3: Substrate-Repair Concrete, this portion of research was aimed at studying the coupling effects of substrate moisture condition and rapid freezing/thawing (FT) conditions on the OTZ of substrate-repair concrete. As discussed in the literature review of this thesis, rapid freezing and thawing of concrete induces microcracks that will coalesce into macrocracks through damage accumulation [26]. The continued degradation of the concrete allows the intrusion of more water, generating a feedback loop that accelerates the damage. The damage created by FT has been demonstrated to reduce the strength (compressive and tensile) and greatly increase porosity [28, 31]. Therefore, this project evaluated the effect substrate moisture condition maintained on resisting damage accelerated by FT. The specimens used for this project were designed to be the same as those utilized in the substrate-repair portion of this thesis. Therefore, the mix design proportions and material properties of *Tables 1* and *2* apply.

5.2 Methods and Procedures

The samples utilized in this experiment were created like the samples utilized in the substrate-repair portion of this thesis. The specimens were batched and allowed to be cured prior to casting the repair material. The substrates were cured 35 days ± 5 days for all moisture conditions. After curing, the substrates were sawcut in half, washed and cleaned of debris material. Afterwards, they were placed in the environmental chamber at the desired relative humidity associated with each moisture condition: SSD (98% RH), Sub-SSD (80% RH), and OD (10% RH). The substrate-repair specimens were allowed to cure for 110-days prior to subjecting them to rapid freezing and thawing. The extended curing period was due to the availability of equipment in the laboratory required for conducting FT experiments. For a complete discussion on batching, to include schematic of the 3”x3”x12” prisms used in this experiment, refer to Section 3.2.

To generate the rapid freezing and thawing environment, ASTM C666 requires specimens to fluctuate between internal temperatures (IT) of 0°F and 40°F with a deviation of ± 3°F. Once the IT has been achieved, the IT shall remain constant for twice the amount of time necessary to reach the desired IT. Oftentimes, this experiment is conducted using a commercially available freeze/thaw cabinet that is specifically designed for the method, but at the time of this thesis, no cabinet was available. Therefore, it was decided to employ the use of the Cincinnati Sub Zero ZPH-16-3.5-3.5-SC/AC environmental chamber to simulate rapid freezing and thawing conditions. Prior to testing any substrate-repair concrete samples, efforts needed to be completed to determine the time required to achieve the IT specifications outlined in ASTM C666. Therefore, a concrete sample was batched with the inclusion of a thermocouple. The sample was placed in the environmental chamber and monitored as the chamber fluctuated between cooling and heating periods. After several temperature fluctuations, it was determined that it took approximately 30 ± 3 minutes for the IT temperatures to reach desired ranges. Once this timeframe was established, the environmental chamber was programmed. The chamber was programmed to complete one FT cycle in 210 minutes. This allowed the following allocation of time for one cycle:

- Cooling period: 35 minutes to achieve desired IT (0°F ± 3°F). 70 minutes to remain at IT.
- Heating period: 35 minutes to achieve desired IT (40°F ± 3°F). 70 minutes to remain at IT.

Literature reviewed for this thesis has identified a reduction in strength after only one FT cycle [31]. With FT damage occurring almost immediately after rapid freezing and thawing, it was decided to subject the substrate-repair specimens to a total of 20 FT cycles. Additionally, to evaluate the loss of compressive strength after the FT cycles, plain substrate cylinders were placed in the environmental chamber. These cylinders will be tested following 20 FT cycles and will be compared with cylinders not subjected to FT cycling.

5.3 Results and Discussion

After completing 20 FT cycles, the specimens were removed from the environmental chamber and inspected for any visible FT damage. *Figures 71, 72, 73, and 74* display the samples after removal from the environmental chamber.

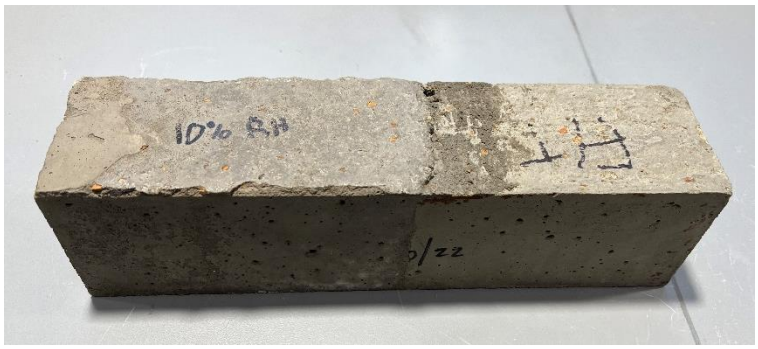

Figure 71: 10% RH Prism after FT

Figure 72: 98% RH Prism after FT

Figure 73: Substrate Cylinder after FT (Top)

Figure 74: Substrate Cylinders after FT (Side)

The images above display no apparent surficial damage from the FT cycles on any of the samples. To evaluate the internal microstructure damage, compressive and flexural strength testing was conducted according to ASTM C39 and ASTM C293 [40, 42]. The average results of the compressive strength testing are presented in *Table 15*.

Table 15: Compressive Strength after FT

Sample Conditions	Average Compressive Strength (psi)	Standard Deviation (psi)
Non-Freeze/Thaw	5,140	127
Freeze/Thaw	4,640	325

The results in *Table 15* indicate that after 20 FT cycles there was an almost 10% reduction in compressive strength. This reduction in compressive strength is in agreement with published literature evaluating the loss of strength due to repeated freezing and thawing [31]. After evaluating the compressive strength of the specimens, ASTM C293 was performed on the 3”x3”x12” prisms. The results of this testing are presented in *Table 16*, with average values presented in *Table 17*.

Table 16: 3-Point Flexural Testing Results after Freeze/Thaw

Specimen	Test	Max Load (lbf)	Span Length (in)	Specimen Depth (in)	Specimen Width (in)	Modulus of Rupture (psi)
98% RH	1	285.1	9.25	3.05	3.15	130
	2	394.3	9.25	3.05	3.15	185
	3	147.6	9.25	3.00	3.05	70
	Average	**275.7**	-	-	-	**130**
	Std. Dev.	-	-	-	-	**55**
80% RH	1	574.1	9.25	3.00	3.10	280
	2	336.1	9.25	3.00	3.20	155
	3	324.3	9.25	3.00	3.10	160
	Average	**411.5**	-	-	-	**195**
	Std. Dev.	-	-	-	-	**70**
10% RH	1	291.9	9.25	3.00	3.05	140
	2	291.6	9.25	3.10	3.05	145
	Average	**291.7**	-	-	-	**140**
	Std. Dev.	-	-	-	-	**5**

Table 17: Freeze/Thaw Flexural Testing Comparison

Specimen	Avg. Max Load (lbf)	Avg. Modulus of Rupture (psi)
98% RH	275.7	130
80% RH	411.5	195
10% RH	291.7	140

After analyzing the results presented in *Table 17*, no positive relationship between substrate moisture condition and resistance to freeze/thaw damage can be formed. The 80% RH moisture condition experienced the highest flexural strength after repeated FT cycles, whereas the least performing condition was the 98% RH. Although the results of the 80% RH samples may seem to suggest increased performance for this moisture condition, this condition also presented the largest standard deviation (70 psi). Two of the three samples in this moisture condition experienced maximum peak loads just below 340 lbf, with one sample demonstrating a maximum peak load of 574.1 lbf. This peak load may indicate an outlier in the dataset and this sort of variation in results cannot lead to an accurate conclusion of increased flexural

strength for this moisture condition. Additionally, it is important to note that for the 10% RH moisture condition only two samples were tested due to early adhesion issues. These adhesions issues resulted in one specimen for the FT testing failing to properly bond with substrate material. In Section 3.2, there is an in-depth discussion of the adhesion issues experienced in this study. Ultimately, it is believed that surface roughness, low substrate moisture condition, and increased voids in the repair material are suspected reasons for the adhesion issues.

To accurately compare the damage due to rapid freezing and thawing, the results of the 3-point flexural tests from this chapter are compared with the 3-point flexural tests results from Section 3.2. The comparison of these results is presented in *Table 18.*

Table 18: Freeze/Thaw Flexural Testing Results Comparison

Environmental Condition	Specimen	Avg. Max Load (lbf)	Avg. Modulus of Rupture (psi)
Freeze/Thaw	98% RH	275.7	130
	80% RH	411.5	195
	10% RH	291.7	140
Non-Freeze/Thaw	98% RH	693.2	340
	80% RH	903.2	430
	10% RH	1066.5	500

After reviewing the results presented in *Table 18*, a significant reduction in flexural strength was observed in all specimens after 20 FT cycles. For all substrate moisture conditions evaluated, flexural strength was decreased by over 50%. This reduction in flexural strength seems to agree with published literature that observed decreases in strength of 33% and 25% for w/c ratios of 0.45 and 0.32 after 20 FT cycles [32]. However, these reductions appear to be less severe than the reductions observed in this study. We believe this is due to the OTZ between the substrate-repair material and the performance of the OTZ in resisting FT damage. Literature reviewed for this thesis has indicated that initial cracks formed along an ITZ will propagate along the length of the ITZ during FT cycling and will therefore increase degradation in this region [29]. Additionally, the same study noted the ITZ grew at rate 2.5 times greater than the control group when exposing samples to the coupling effects of loading and freeze/thaw cycling.

Furthermore, the moisture condition that demonstrated the greatest reduction in flexural strength was the 10% RH samples. These samples exhibited a 72% reduction in flexural strength after 20 FT cycles. This significant reduction in flexural strength may be the result of two published conclusions, 1) increased voids in the OTZ of dry substrates, and 2) isolated voids are connected during FT cycles [28, 41]. Since the 10% RH samples would maintain an increased void content, it would follow that after repeated FT cycles, they would develop a more significant reduction in strength.

5.4 Conclusions

After conducting 20 FT cycles on substrate-repair specimens with various substrate moisture conditions, no positive relationship between moisture condition and FT resistance can be made. There appears to be a slight improvement in flexural strength as the substrate moisture condition decreases. This increase may potentially be attributed to a decrease in locally available water along the OTZ, resulting in less available water to freeze and thaw during FT cycles. However, if such a relationship were to exist, the 10% RH specimens would be expected to exhibit higher strengths than the 80% RH samples. Since these results were not observed, no such conclusion may be made. The only significant conclusion resulting from the tests would be the significant decrease in flexural strength following repeated FT cycles. The observed reduction in flexural strength after FT appears to have been greater than what is seen after FT of specimens made of one homogenous sample. That is, the reductions in flexural strength of substrate-repair concrete seem to be greater than plain bulk samples. This would highlight the significance of the OTZ on strength properties.

5.5 Future Work

To expand on the observations in this study, transmission X-ray microscopy can be performed to evaluate the transport properties of the substrate-repair OTZ after repeated freezing and thawing cycles. Samples can be exposed to the same number of FT cycles, cored along the interface, and ponded with a 0.6 mol/L KI solution as discussed in Chapter 4 of this thesis. This would allow the researcher to evaluate the effects of repeated FT cycles on the transport properties of the material. Furthermore, additional

strengths tests like slant shear and pull-off testing can be performed to identify any relationship between substrate moisture condition and strength properties. As research reviewed for this thesis has identified, optimum substrate moisture condition is contingent on the parameter or property being measured. Therefore, evaluating other material properties would be beneficial.

6. Conclusions and Future Work

After conducting the experiments outlined in this thesis, no positive relationship between substrate moisture condition and strength could be made. There does appear to be an increase in chloride ion penetration risk for drier substrates. As discussed, this may be due to the increase in porosity along the overlay transition zone associated with drier substrates. Additional experiments evaluating flexural strength would need to be performed to identify any correlation between moisture condition and flexural strength. The 3-point flexural testing results presented in this thesis seem to indicate an improvement in strength for drier substrates. This was attributed to a lowering of the local w/c ratio as the substrate absorbs water from the repair material. However, due to limited sample sizes this relationship cannot be confidently established. In future research, two recommendations are provided: 1) abrade substrate surfaces to increase mechanical interlock between substrate and repair materials and 2) increase water availability on the substrate surface to make the significance of moisture condition more apparent. To increase water availability, it is recommended to either utilize an alternative form of conditioning (like ponding or physically saturating surfaces) or to greatly extend the conditioning time in the environmental chamber. In this study, samples were conditioned for 18 ± 2 hours. In future research, this period may be extended to upwards of 7 days to provide greater time for the samples to achieve their desired relative humidity. It is presumed that increasing the conditioning period may allow for greater water availability along substrate surfaces during batching of repair material.

An interesting observation in this study was the increase in the rate of degradation in substrate-repair specimens subjected to rapid freezing and thawing. The results presented in this thesis display a significant decrease in flexural strength of substrate-repair samples subjected to freezing and thawing when compared to homogenous concrete samples subjected to the same conditions. These results would highlight the importance of the OTZ and may indicate an increase rate of degradation along this zone. Future research may attempt to characterize this degradation through transmission X-ray microscopy and evaluating the diffusivity of chloride ions. Such analysis may be able to quantify the penetration risk

along the OTZ and would be an important statistic when assessing optimum substrate moisture condition for samples subjected to rapid freezing and thawing conditions.

In addition to completing the construction of the CHIP system, future research may aim to enhance the design to provide the capability of scanning larger samples. These samples may be of cement mortar or concrete cores. In doing so, the samples scanned in the CHIP system may be more reflective of the types of specimens retrieved from concrete elements in the field. Furthermore, the CHIP system can be employed to conduct TXM experiments on the OTZ of substrate-repair samples subjected to normal environmental conditions. The results of the TXM experiments may be coupled with RCPT data to provide a more complete picture of the substrate moisture conditions effect on diffusivity.

Appendix A

Figures 75, 76, 77, 78, and 79 display the computer-aided design (CAD) drawings with dimensions for the XCT stage and filter holder. The drawings display important dimensions regarding the PVC nut insert, screw hole diameters, and size of filter insert.

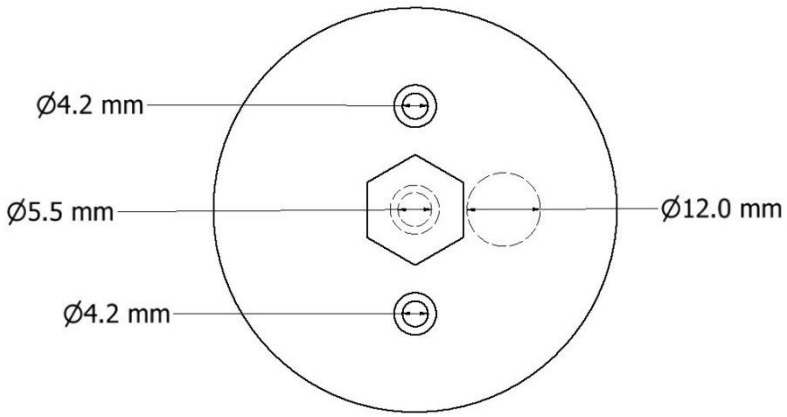

Figure 75: XCT Stage (Top)

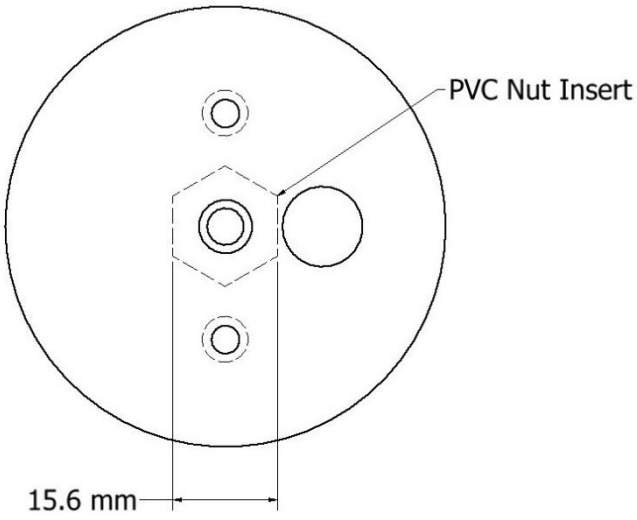

Figure 76: XCT Stage (Bottom)

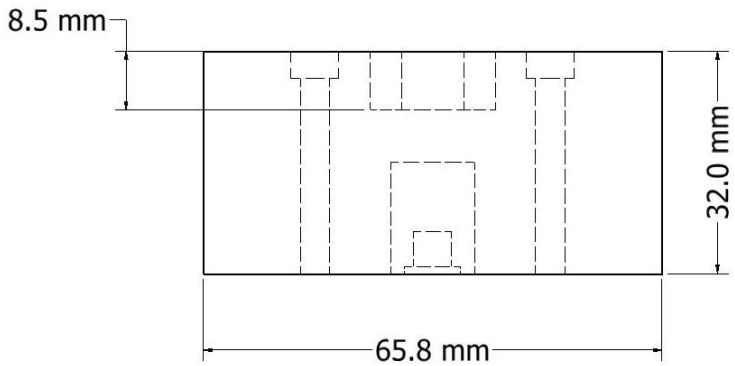

Figure 77: XCT Stage (Side)

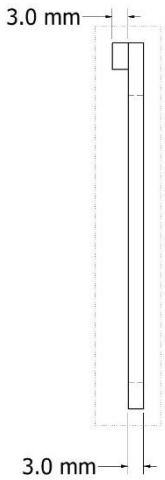

Figure 78: Filter Holder (Side)

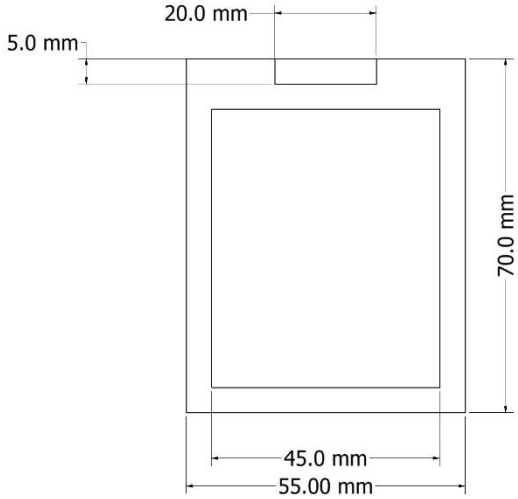

Figure 79: Filter Holder (Front)

References

[1] H. Beushausen, B. Höhlig, M. Talotti, The influence of substrate moisture preparation on bond strength of concrete overlays and the microstructure of the otz, Cement and Concrete Research, 92 (2017) 84-91.

[2] K.L. Scrivener, A.K. Crumbie, P. Laugesen, The interfacial transition zone (itz) between cement paste and aggregate in concrete, Interface Science, 12 (2004) 411-421.

[3] M.G. Alexander, L. Courard, B. Bissonnette, A. Garbacz, A.M. Vaysburd, K.F. von Fay, H. Beushausen, F. Dehn, P. Moyo, Guidelines for concrete surface preparation: 10 years research and experience, MATEC Web of Conferences, 199 (2018).

[4] H. Mefteh, O. Kebaïli, H. Oucief, L. Berredjem, N. Arabi, Influence of moisture conditioning of recycled aggregates on the properties of fresh and hardened concrete, Journal of Cleaner Production, 54 (2013) 282-288.

[5] A.S. Brand, J. Roesler, Interfacial transition zone of cement composites with recycled concrete aggregate of different moisture states, Advanced Civil Engineering Materials, 7 (2018) 87-102.

[6] M.B. Leite, P.J.M. Montiero, Microstructural analysis of recycled concrete using x-ray microtomography, Cement and Concrete Research, 81 (2016) 38-48.

[7] H. Beushausen, The influence of concrete substrate preparation on overlay bond strength, Magazine of Concrete Research, 62 (2010) 845-852.

[8] A.M. Vaysburd, B. Bissonnette, M.M. Thomassin, K.F. von Fay, S.J. Harrell, B. Robertson, Concrete substrate moisture requirements for effective concrete repairs, (2016).

[9] Z. Hashin, P.J.M. Monteiro, An inverse method to determine the elastic properties of the interphase between the aggregate and the cement paste, Cement and Concrete Research, 32 (2002) 1291-1300.

[10] D.P. Bentz, I. De la Varga, J.F. Munoz, R.P. Spragg, B.A. Graybeal, D.S. Hussey, D.L. Jacobson, S.Z. Jones, J.M. LaManna, Influence of substrate moisture state and roughness on interface microstructure and bond strength: Slant shear vs. Pull-off testing, Cem Concr Compos, 87 (2018) 63-72.

[11] L. Courard, J.F. Lenaers, F. Michel, A. Garbacz, Saturation level of the superficial zone of concrete and adhesion of repair systems, Construction and Building Materials, 25 (2011) 2488-2494.

[12] M. Alexander, A. Bentur, S. Mindess, Durability of concrete: Design and construction, CRC Press 2017.

[13] Corrosion costs and preventive strategies in the united states, NACE International, 2002.

[14] ASCE, Asce report card, 2021.

[15] AASHTO, Aashto t 358 - standard method of test for surface resistivity indication of concrete's ability to resist chloride ion penetration, 2017.

[16] K.P.V. Robles, D.-W. Kim, J.-J. Yee, J.-W. Lee, S.-H. Kee, Electrical resistivity measurements of reinforced concrete slabs with delamination defects, Sensors, 20 (2020) 7113.

[17] ASTM, C1202 - standard test method for electrical indication of concrete's ability to resist chloride ion penetration, ASTM International, West Conshohocken, PA, 2022.

[18] ASTM, C1556 - standard test method for determining the apparent chloride diffusion coeffecient of cementitious mixtures by bulk diffusion, ASTM International, West Conshohocken, PA, 2016.

[19] Nt build 492: Chloride migration coefficient from non-steady-state migration experiments, Nordtest, 1999.

[20] I.S. Darma, T. Sugiyama, M.A.B. Promentilla, Application of x-ray ct to study diffusivity in cracked concrete through the observation of tracer transport, Journal of Advanced Concrete Technology, 11 (2013) 266-281.

[21] G. Sant, J. Weiss, Using x-ray absorption to assess moisture movement in cement-based materials, Journal of ASTM International 6(2009).

[22] A. Behravan, M.T. Ley, A. Rywelski, N. Berke, Changes in the rate of ion penetration of alternative cementitious materials with time, Materials & Design, 197 (2021).

[23] M. Khanzadeh Moradllo, Q. Hu, M.T. Ley, Using x-ray imaging to investigate in-situ ion diffusion in cementitious materials, Construction and Building Materials, 136 (2017) 88-98.

[24] S. Kang, M. Tyler Ley, A. Behravan, Predicting ion diffusion in fly ash cement paste through particle analysis, Construction and Building Materials, 272 (2021).

[25] T.M. Ley, D. Cook, A. Behravan, Q. Hu, Using medical x-ray machine to determine the service life of concrete, Transportation Research Board (TRB), 2019.

[26] R. Wang, Z. Hu, Y. Li, K. Wang, H. Zhang, Review on the deterioration and approaches to enhance the durability of concrete in the freeze–thaw environment, Construction and Building Materials, 321 (2022).

[27] Y. Şahin, Y. Akkaya, M.A. Taşdemir, Effects of freezing conditions on the frost resistance and microstructure of concrete, Construction and Building Materials, 270 (2021).

[28] Z. Tian, X. Zhu, X. Chen, Y. Ning, W. Zhang, Microstructure and damage evolution of hydraulic concrete exposed to freeze–thaw cycles, Construction and Building Materials, 346 (2022).

[29] X. Yang, A. Shen, Y. Guo, S. Zhou, T. He, Deterioration mechanism of interface transition zone of concrete pavement under fatigue load and freeze-thaw coupling in cold climatic areas, Construction and Building Materials, 160 (2018) 588-597.

[30] C. Yi, S.L. Lai, H.G. Zhu, S.H. Yan, J.X. Liu, X. Dong, Freeze-thawing damage model of new-to-old concrete with different rough interfaces, Applied Mechanics and Materials, 405-408 (2013) 2707-2714.

[31] A.J.K. Komar, A.J. Boyd, Evaluating freeze-thaw deterioration with tensile strength, Material Science Engineering, (2017).

[32] W. Sun, Y.M. Zhang, H.D. Yan, R. Mu, Damage and damage resistance of high strength concrete under the action of load and freeze-thaw cycles, Cement and Concrete Research, 29 (1999) 1519-1523.

[33] A.C.I. Committee, Standard practice for selecting proportions for structural lightweight concrete, ACI Materials Journal, 87 (1990) 638-651.

[34] S. Lane, Fhwa ltbp summary - current information on the use of overlays and sealers, in: F.H.A. (FHWA) (Ed.), 2017.

[35] G. Fick, J. Gross, M.B. Synder, D. Harrington, Guide to concrete overlays, National Concrete Pavement Technology Center, 2021.

[36] ASTM, C127 - standard test method for relative density (specific gravity) and absorption of coarse aggregate, ASTM International, West Conshohocken, PA, 2015.

[37] ASTM, C128 - standard test method for relative density (specific gravity) and absorption of fine aggregate, ASTM International, West Conshohocken, PA, 2015.

[38] ASTM, C192 - standard practice for making and curing concrete test specimens in the laboratory, ASTM International, West Conshohocken, PA, 2019.

[39] ASTM, C143 - standard test method for slump of hydraulic-cement concrete, ASTM International, West Conshohocken, PA, 2020.

[40] ASTM, C39 - standard test method for compressive strength of cylindrical concrete specimens, ASTM International, West Conshohocken, PA, 2021.

[41] M. Lukovic, G. Ye, Effect of moisture exchange on interface formation in the repair system studied by x-ray absorption, Materials (Basel), 9 (2015).

[42] ASTM, C293 - standard test method for flexural strength of concrete (using simple beam with center-point loading), ASTM International, West Conshohocken, PA, 2016.

[43] ASTM, C78 - standard test method for flexural strength of concrete (using simple beam with third-point loading), ASTM International, West Conshohocken, PA, 2022.

[44] S.P. Shah, Rilem draft recommendations for determination of fracture parameters of plain concrete using three-point bend tests, Materials and Structures, 23 (1990) 457-460.

[45] P. Gao, J. Wei, T. Zhang, J. Hu, Q. Yu, Modification of chloride diffusion coefficient of concrete based on the electrical conductivity of pore solution, Construction and Building Materials, 145 (2017) 361-366.

[46] J. Marchand, A. Delagrave, Influence of itz on ionic diffusion and leaching.

[47] ASTM, C305 - standard practice for mechanical mixing of hydraulic cement pastes and mortars of plastic consistency, ASTM International, West Conshohocken, PA, 2020.